Eighth-order QED contribution to the anomalous magnetic moment of the muon

T. Kinoshita, B. Nizic,* and Y. Okamoto†
Newman Laboratory of Nuclear Studies, Cornell University, Ithaca, New York 14853
(Received 27 September 1989)

We report a calculation of the eighth-order QED contribution to the muon anomalous magnetic moment $a_\mu^{(8)}$ coming from 469 Feynman diagrams, all of which contain electron loops of vacuum-polarization type and/or light-by-light scattering type. Our result is $126.92(41)(\alpha/\pi)^4$. The error represents the estimated accuracy (90% confidence limit) of the required numerical integration. We also report an estimate of the tenth-order contribution to a_μ. Combining these with the lower-order results and the latest theoretical value for the electron anomaly a_e, we find that the QED contribution to the muon anomaly is given by $a_\mu^{\rm QED}=1\,165\,846\,947(46)(28)\times10^{-12}$, where the first error is an estimate of theoretical uncertainty and the second reflects the measurement uncertainty in α. Including the hadronic and electroweak contributions, the best theoretical prediction for a_μ available at present is $a_\mu^{\rm theory}=116\,591\,920\,(191)\times10^{-11}$, where the error comes predominantly from the hadronic contribution.

I. INTRODUCTION AND SUMMARY

The anomalous magnetic moment of the muon a_μ provides one of the most stringent tests of the renormalization program of the standard model, the unified electroweak sector in particular. This is in strong contrast to the anomalous magnetic moment of the electron a_e, which is rather insensitive to strong and weak interactions, and hence offers the best testing ground for the "pure" quantum electrodynamics.

Much of the theoretical analysis is identical for electrons and muons except that the effect of the electron on a_μ and that of the muon on a_e, via vacuum polarization, are quite asymmetric. The electron, being much less massive than the muon, cannot readily create a virtual muon-antimuon pair. Thus muons (and all heavier particles) have little observable effects on a_e. The muon, on the other hand, can create a virtual electron-positron pair with relative ease. Indeed, in the fourth and higher orders, diagrams containing electron loops dominate. Similarly, the effects of strong and weak interactions are much more important in a_μ than in a_e.

In testing the theoretical prediction for a_μ experimentally, it is crucial to know all these contributions precisely. We have therefore carried out an extensive calculation of terms contributing to a_μ, and managed to reduce the theoretical error from the previous value of 10×10^{-9} to 2×10^{-9}, which is of the same order of magnitude as the weak-interaction effect on a_μ. A preliminary result of this calculation was reported in Ref. 1. It has provided a strong motivation for the new muon $g-2$ experiment E821 which is in progress at the Brookhaven National Laboratory. When this experiment and associated experiments needed to improve the hadronic contribution to a_μ are completed, our theoretical results will enable us to test the prediction of the standard model at the one-loop level. In addition, it provides useful constraints on possible muon internal structure[2] as well as supersymmetric and other theories.[3]

In this paper we present a detailed account of our calculation of the eighth-order QED contribution to a_μ. In addition we report an estimate of the tenth-order QED contribution. The long delay in the publication of the eighth-order result was caused by the unavailability, until the last couple of years, of computing power which could adequately handle some of the huge integrals involved. Our evaluation of the hadronic effect on a_μ was reported elsewhere.[4]

The QED diagrams contributing to the anomalous magnetic moment of a charged lepton (electron, muon, or tauon) can be divided into three groups: (i) diagrams containing only one kind of lepton; (ii) diagrams containing two kinds of leptons; and (iii) diagrams containing all three leptons. The anomaly for a lepton of mass m_1, being a dimensionless quantity, can be expressed in the general form

$$a = A_1 + A_2(m_1/m_2) + A_2(m_1/m_3) + A_3(m_1/m_2, m_1/m_3)\ , \tag{1.1}$$

where m_2 and m_3 are the masses of other leptons. For the electron and the muon we have

$$a_e = A_1 + A_2(m_e/m_\mu) + A_2(m_e/m_\tau) + A_3(m_e/m_\mu, m_e/m_\tau)\ , \tag{1.2}$$

$$a_\mu = A_1 + A_2(m_\mu/m_e) + A_2(m_\mu/m_\tau) + A_3(m_\mu/m_e, m_\mu/m_\tau)\ . \tag{1.3}$$

The renormalizability of QED guarantees that A_1, A_2, and A_3 can be expanded in power series in α/π with finite calculable coefficients:

$$A_i = A_i^{(2)}\left(\frac{\alpha}{\pi}\right) + A_i^{(4)}\left(\frac{\alpha}{\pi}\right)^2 + A_i^{(6)}\left(\frac{\alpha}{\pi}\right)^3 + \cdots\ , \quad i=1,2,3\ . \tag{1.4}$$

The value of A_1 has been evaluated to the eighth order.[5] Clearly, $A_2^{(2)}=A_3^{(2)}=A_3^{(4)}=0$ since there is no Feynman diagram that contributes to them.

Before discussing the muon anomaly a_μ, let us briefly comment on A_2 and A_3 of the electron anomaly a_e. In order to obtain the precision needed at present, it is sufficient to calculate $A_2^{(4)}(m_e/m_\mu)$ because of smallness of the ratios m_e/m_μ and m_e/m_τ. This contribution arises from the diagram obtained by inserting a muon vacuum-polarization loop in the second-order electron vertex. The result is known analytically[6] and is given by

$$A_2^{(4)}(m_e/m_\mu)=\frac{1}{45}\left[\frac{m_e}{m_\mu}\right]^2+O\left[\left[\frac{m_e}{m_\mu}\right]^4\ln\frac{m_\mu}{m_e}\right]$$
$$=5.198\times10^{-7}\ . \tag{1.5}$$

The term $A_2^{(4)}(m_e/m_\tau)$ is $(m_\mu/m_\tau)^2$ times smaller than (1.5) and can be ignored at present. The term $A_3^{(6)}(m_e/m_\mu,m_e/m_\tau)$ is of order $(\alpha/\pi)^3(m_e/m_\mu)^2(m_e/m_\tau)^2$, and is negligible, too. Throughout this paper we use the lepton mass values $m_e=0.510\,999\,06(15)$ MeV/c^2, $m_\mu=105.658\,39(6)$ MeV/c^2, and $m_\tau=1\,784.1(+2.7/-3.6)$ MeV/c^2 listed in Ref. 7.

Let us now summarize the results for the muon anomaly a_μ, which are radically different from that of the electron anomaly a_e because of the large mass ratio m_μ/m_e.

The fourth-order term $A_2^{(4)}(m_\mu/m_e)$ is known analytically and, up to terms of the order $(m_e/m_\mu)^2$, given by[8]

$$A_2^{(4)}(m_\mu/m_e)=\frac{1}{3}\ln\frac{m_\mu}{m_e}-\frac{25}{36}+\frac{\pi^2}{4}\frac{m_e}{m_\mu}$$
$$-4\left[\frac{m_e}{m_\mu}\right]^2\ln\frac{m_\mu}{m_e}$$
$$+3\left[\frac{m_e}{m_\mu}\right]^2+O\left[\left[\frac{m_e}{m_\mu}\right]^3\right]$$
$$=1.094\,259\,6\ldots\ . \tag{1.6}$$

The contribution to $A_2^{(6)}(m_\mu/m_e)$ arises from 24 sixth-order Feynman diagrams. These include 18 diagrams containing electron vacuum-polarization loops and six diagrams containing light-by-light scattering subdiagrams. The contribution of the first group is known analytically up to terms of order m_e/m_μ and also numerically[9] while that of the second group is known only by numerical means.[1,10] Unfortunately, these early results are not accurate enough for our purpose. In any case, however, a better evaluation of these quantities is needed in carrying out the calculation of the eighth-order contribution. Thus, we have reevaluated them using the adaptive Monte Carlo integration routine VEGAS (Ref. 11). The new values are[12]

$$\begin{aligned}&A_2^{(6)}(m_\mu/m_e;\text{vacuum polarization})=1.920\,0(14)\ ,\\ &A_2^{(6)}(m_\mu/m_e;\text{light-by-light})=20.947\,1(29)\ .\end{aligned} \tag{1.7}$$

The first term consists of several integrals as shown in (2.36). These integrals, all listed in tables in Sec. II, are evaluated using up to 40 iterations with up to 4×10^7 function calls per iteration. The second term, which was reported elsewhere,[12] is obtained by evaluating the integrand at 14×10^7 randomly chosen sampling points each for the first 10 iterations and 28×10^7 sampling points each for subsequent 20 iterations. The latter confirms and improves our earlier result.[1] It agrees with the direct, although much cruder, evaluation of Samuel and Chlouber[13] within their stated errors. However, the error assigned to the extrapolated value given in Ref. 13 must be multiplied by 7 in order to bring it into agreement with (1.7) (Ref. 14). Using the improved values in (1.7) we find that the total sixth-order contribution is given by

$$A_2^{(6)}(m_\mu/m_e)=22.867\,1(33)\ . \tag{1.8}$$

The contribution to $A_2^{(8)}(m_\mu/m_e)$ arises from 469 eight-order Feynman diagrams. After more than four years of extensive numerical work, we have obtained

$$A_2^{(8)}(m_\mu/m_e)=126.92(41)\ . \tag{1.9}$$

An outline of this calculation is given in Sec. II. This result is an order-of-magnitude improvement in precision over the preliminary value 140(6) reported in Ref. 1. The apparent disagreement between the two results is due to an overly optimistic error estimate in the latter caused by insufficient samplings of integrands.

We have also obtained a preliminary value for the tenth-order term $A_2^{(10)}(m_\mu/m_e)$ by evaluating numerically the contribution of the leading 36 diagrams, all of which contain one light-by-light scattering electron loop and two second-order electron vacuum-polarization loops, and making a rough estimate of others:

$$A_2^{(10)}(m_\mu/m_e)=570(140)\ , \tag{1.10}$$

where the uncertainty is an estimated upper bound for the contribution of uncalculated terms. See Sec. III for details.

As for the tauon-loop contribution, the fourth-order term $A_2^{(4)}(m_\mu/m_\tau)$ has the same form as (1.5) with an appropriate change of variables. We find

$$A_2^{(4)}(m_\mu/m_\tau)=7.794(32)\times10^{-5}\ , \tag{1.11}$$

which contributes $421(1)\times10^{-12}$ to a_μ. Higher-order terms of $A_2(m_\mu/m_\tau)$ are about α/π times smaller than (1.11) and hence need not be considered at present.

The lowest-order contribution to $A_3(m_\mu/m_e,m_\mu/m_\tau)$ arises from a sixth-order diagram which is obtained by inserting an electron vacuum-polarization loop and a tauon vacuum-polarization loop in the second-order muon vertex. On numerical integration we find

$$A_3^{(6)}(m_\mu/m_e,m_\mu/m_\tau)=5.24(1)\times10^{-4}\ . \tag{1.12}$$

This contributes 7×10^{-12} to a_μ. The only significant contributions to $A_3^{(8)}(m_\mu/m_e,m_\mu/m_\tau)$ arise from a muon vertex which contains an electron light-by-light scattering subdiagram and a tauon vacuum-polarization loop and another in which the roles of electron and tauon are interchanged. We have evaluated the sum of these contributions numerically:

$$A_3^{(8)}(m_\mu/m_e, m_\mu/m_\tau) = 0.079(3) \ . \tag{1.13}$$

This contribution to a_μ amounts to 2.3×10^{-12}. Contributions to $A_3^{(8)}(m_\mu/m_e, m_\mu/m_\tau)$ from other diagrams are at least an order of magnitude smaller than (1.13) and thus negligible at present.

We are now ready to calculate a_μ. Using the latest value of the fine-structure constant determined in terms of the quantized Hall effect,[15]

$$\alpha^{-1} = 137.035\,997\,9(32) \ , \tag{1.14}$$

one finds from the results (1.5)–(1.13) that

$$a_\mu - A_1 = 6\,194\,817(45)\times10^{-12} \ , \tag{1.15}$$

where the numeral within the parentheses is an estimate of theoretical uncertainty generated by the integration routine. [The uncertainty due to the error in α of (1.14) is less than 0.3×10^{-12} and is completely negligible.] Adding to this the value of A_1 obtained from the calculation of the electron anomaly, which through the eighth order is[16]

$$A_1 = 1\,159\,652\,130\,(8.4)(28)\times10^{-12} \ , \tag{1.16}$$

we find that the pure QED contribution to the muon anomaly is given by

$$a_\mu^{\rm QED} = 1\,165\,846\,947(46)(28)\times10^{-12} \ . \tag{1.17}$$

The first errors in (1.16) and (1.17) are estimates of theoretical uncertainties and the second reflect the measurement uncertainty of α in (1.14).

We note that the theoretical uncertainty in (1.17) is mostly due to that of the α^3 term (1.8). There is no intrinsic difficulty in reducing this error further. This will be attempted in the near future.

In order to compare theory with experiment we must also include hadronic and electroweak contributions. The latest estimate of the hadronic effects (vacuum polarization due to hadrons) including the fourth- and sixth-order contributions, is[4,17]

$$a_\mu^{\rm had} = 703(19)\times10^{-10} \ . \tag{1.18}$$

The one-loop weak-interaction contribution calculated within the framework of the Weinberg-Salam model is[18]

$$a_\mu^{\rm weak} = 195(1)\times10^{-11} \ . \tag{1.19}$$

Here the uncertainty comes mostly from the lack of experimental information on the Higgs-boson mass m_H. If m_H is as light as the present lower limit[19] of 5 GeV/c^2, $a_\mu^{\rm weak}$ will be pushed up to 196×10^{-11}, which is at the upper end of uncertainty in (1.19). For higher masses the Higgs contribution becomes rapidly insignificant, decreasing as m_H^{-2}. The uncertainty in the Weinberg angle[7] has a relatively minor effect, contributing only 0.13×10^{-11} to the error in (1.19). Thus the error limits in (1.19) is strongly asymmetric. Finally we must keep in mind that the effect of two-loop contributions is unknown at present.

Summing up the contributions (1.17) through (1.19), we obtain the overall theoretical prediction for the muon anomaly,

$$a_\mu^{\rm theor} = 116\,591\,920(191)\times10^{-11} \ , \tag{1.20}$$

which is in good agreement with the current experimental values:[20]

$$\begin{aligned} a_{\mu^-}^{\rm expt} &= 1\,165\,937(12)\times10^{-9} \ , \\ a_{\mu^+}^{\rm expt} &= 1\,165\,911(11)\times10^{-9} \ . \end{aligned} \tag{1.21}$$

As a consequence of this work we have reduced the theoretical QED-type uncertainty in a_μ to less than 3% of the uncertainty in the hadronic term (1.18). The latter happens to be of the same order of magnitude as the electroweak effect (1.19). Thus, for experimental detection of the electroweak effect, it is necessary to improve the accuracy of the hadronic contribution (1.18) by a factor of 5 or more. This requires more accurate measurements of R, the ratio of hadron production cross section and muon-pair production cross section in e^+e^- collisions. See Ref. 21 for a discussion of feasibility of such an improvement. A new experiment is in progress at the Brookhaven National Laboratory to measure the a_μ about 20 times more accurately than (1.21). Together with improved measurements of R, this will enable us to detect the electroweak effect (1.19) within the uncertainty of 30% or better.

The rest of the paper is organized as follows. In Sec. II we give an outline of our method for calculating $A_2^{(8)}(m_\mu/m_e)$ and present the results. A preliminary evaluation of the tenth-order contribution $A_2^{(10)}(m_\mu/m_e)$ is described in Sec. III. In the Appendix we compare some of our numerical results with the corresponding approximate results obtained using the renormalization-group technique and evaluate the terms left undetermined by the latter. This may someday become relevant in the theoretical study of higher-order terms.

II. OUTLINE OF THE METHOD AND RESULTS OF CALCULATION

For simplicity we omit the factor $(\alpha/\pi)^4$ throughout this section.

In the eighth order there are altogether 469 Feynman diagrams contributing to the term $A_2(m_\mu/m_e)$ of (1.3). They all have subdiagrams of the vacuum-polarization type and/or light-by-light scattering type and can be classified into four (gauge-invariant) groups.

Group I. Second-order vertex diagrams containing vacuum-polarization loops of second, fourth, and sixth orders. This group consists of 49 diagrams. Typical diagrams are shown in Fig. 1(a).

Group II. Fourth-order vertex diagrams containing vacuum-polarization loops of second and fourth orders. This group consists of 90 diagrams. Typical diagrams are shown in Fig. 1(b).

Group III. Sixth-order vertex diagrams containing vacuum-polarization loop of second order. This group consists of 150 diagrams. A typical diagram is shown in Fig. 1(c).

Group IV. Vertex diagrams containing a light-by-light

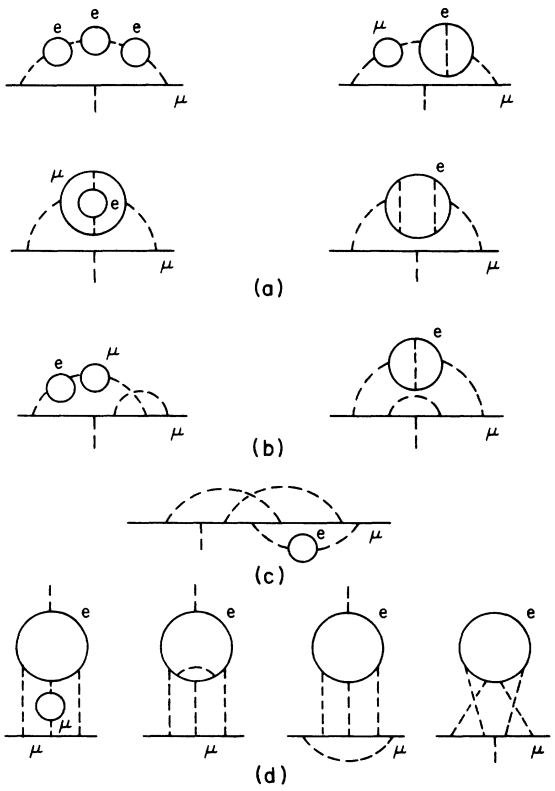

FIG. 1. Typical eighth-order vertex diagrams from the four groups contributing to a_μ.

scattering subdiagram with further radiative corrections of various kinds. This group consists of 180 diagrams. Typical diagrams are shown in Fig. 1(d).

Group I

These diagrams can be classified further into the following gauge-invariant subgroups.

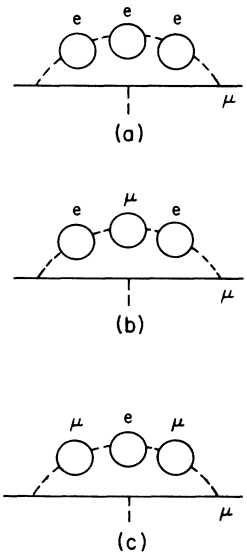

FIG. 2. Three of the diagrams contributing to subgroup I(a).

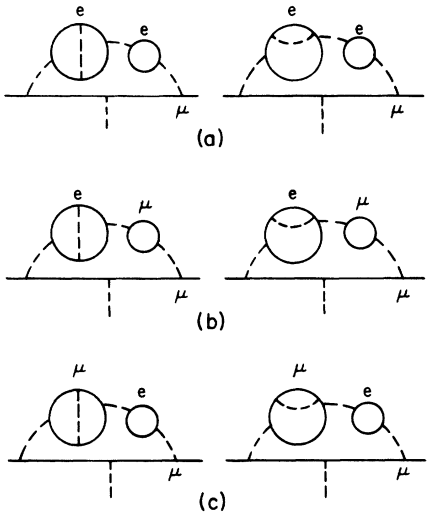

FIG. 3. Six of the diagrams contributing to subgroup I(b).

Subgroup I(a). Diagrams obtained by inserting three second-order vacuum-polarization loops in a second-order vertex. Seven diagrams belong to this subgroup. Three are shown in Fig. 2. The other four are obtained from diagrams of Figs. 2(b) and 2(c) by permuting electron and muon loops along the photon line.

Subgroup I(b). Diagrams obtained by inserting one second-order and one fourth-order vacuum-polarization loops in a second-order vertex. Eighteen diagrams belong to this subgroup. Six are shown in Fig. 3.

Subgroup I(c). Diagrams containing two closed fermion loops one within the other. There are nine diagrams that belong to this subgroup. Six of them are shown in Fig. 4.

Subgroup I(d). Diagrams obtained by insertion of sixth-order (single electron loop) vacuum-polarization

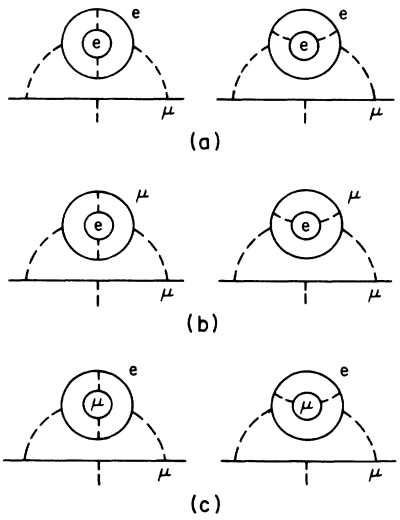

FIG. 4. Six of the diagrams contributing to subgroup I(c).

subdiagrams in a second-order muon vertex. Fifteen diagrams belong to this subgroup. Eight are shown in Fig. 5. Each of A, C, D, E, and F and the time-reversed diagram for E has a charge-conjugated counterpart.

The evaluation of contributions of subgroups I(a) and I(b) is greatly facilitated by the analytic formulas available for the second- and fourth-order Källén-Lehmann spectral representations of the renormalized photon propagator.

Following the discussion in Sec. II of Ref. 22, the contribution to a_μ from the diagram obtained by sequential insertion of m kth-order electron and n lth-order muon vacuum-polarization loops into a second-order vertex is given by

$$a=\int_0^1 dy(1-y)\left[\int_0^1 ds\frac{\rho_k(s)}{1+\frac{4}{1-s^2}\frac{1-y}{y^2}\left[\frac{m_e}{m_\mu}\right]^2}\right]^m \times\left[\int_0^1 dt\frac{\rho_l(t)}{1+\frac{4}{1-t^2}\frac{1-y}{y^2}}\right]^n , \tag{2.1}$$

where ρ_k is the kth-order spectral function. Explicit forms of ρ_2 and ρ_4 are given by Eqs. (2.9) and (2.10) of Ref. 22.

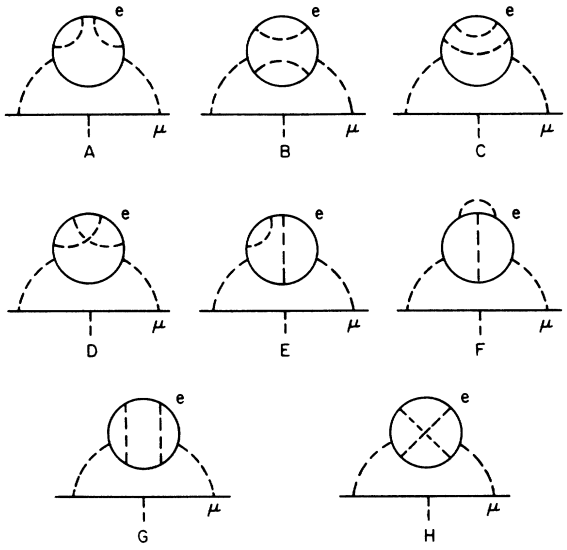

FIG. 5. Eighth-order vertices obtained by insertion of sixth-order (single electron loop) vacuum-polarization diagrams in a second-order muon vertex.

As a special case of (2.1) the contribution of the diagram in Fig. 2(a) can be written as

$$a[\text{Fig. 2(a)}]=\int_0^1 dy(1-y)\left[\int_0^1 ds\frac{\rho_2(s)}{1+\frac{4}{1-s^2}\frac{1-y}{y^2}\left[\frac{m_e}{m_\mu}\right]^2}\right]^3 . \tag{2.2}$$

The contributions of the diagrams in Figs. 2(b) and 2(c) are given by similar expressions. Evaluating these integrals numerically using the integration routine RIWIAD (Ref. 23) with 1.6×10^5 subcubes and 12 iterations, we have found

$$a[\text{Fig. 2(a)}]=7.223\,7(13) , \tag{2.3}$$

$$a[\text{Fig. 2(b)}]=0.494\,2(2) , \tag{2.4}$$

$$a[\text{Fig. 2(c)}]=0.028\,0(1) . \tag{2.5}$$

Thus the total contribution of the diagrams of subgroup I(a) is

$$a^{(8)}_{\text{I(a)}}=7.745\,9(13) . \tag{2.6}$$

The contribution of the diagrams shown in Fig. 3(a) is given by

$$a[\text{Fig. 3(a)}]=2\int_0^1 dy(1-y)\int_0^1 ds\frac{\rho_2(s)}{1+\frac{4}{1-s^2}\frac{1-y}{y^2}\left[\frac{m_e}{m_\mu}\right]^2}\int_0^1 dt\frac{\rho_4(t)}{1+\frac{4}{1-t^2}\frac{1-y}{y^2}\left[\frac{m_e}{m_\mu}\right]^2} . \tag{2.7}$$

The contributions of Figs. 3(b) and 3(c) are similar. Numerical integration by RIWIAD using 1.6×10^5 subcubes and 10 iterations gives

$$a[\text{Fig. 3(a)}]=7.128\,9(23) , \tag{2.8}$$

$$a[\text{Fig. 3(b)}]=0.119\,5(1) , \tag{2.9}$$

$$a[\text{Fig. 3(c)}]=0.333\,7(1) . \tag{2.10}$$

Summing up the values (2.8)–(2.10), one finds for the subgroup I(b) the result

$$a^{(8)}_{\text{I(b)}}=7.582\,1(23) . \tag{2.11}$$

In order to evaluate the contribution to a_μ coming from the nine Feynman diagrams of subgroup I(c), we make use of the parametric integral representation of the

sixth-order QED vacuum-polarization terms obtained in Ref. 24. These contributions can be written in the form

$$a^{(8)}_{\mathrm{I(c)}} = \sum_{(l_1,l_2)} \Delta M^{(l_1,l_2)}_{2,P(P_4,P_2)} + \text{residual renormalization terms} , \quad (2.12)$$

where

$$(l_1,l_2)=(e,e),\ (\mu,e),\ \text{or}\ (e,\mu) ,$$

and

$$\Delta M^{(l_1,l_2)}_{2,P(P_4,P_2)} = \Delta M^{(l_1,l_2)}_{2,P(P_{4a},P_2)} + \Delta M^{(l_1,l_2)}_{2,P(P_{4b},P_2)} \quad (2.13)$$

are finite integrals obtained by the K_S renormalization procedure described in Ref. 22. The suffix P_2 stands for the second-order vacuum-polarization diagram while P_4 represents the complete fourth-order vacuum polarization, which receives contributions from two distinct diagrams P_{4a} and P_{4b}: $P_4=P_{4a}+P_{4b}$. For the meaning of other notations see Ref. 22. Terms appearing on the right-hand side of (2.12) are finite, numerically calculable integrals given by Eqs. (4.2) and (4.6) of Ref. 22, modified appropriately to account for different arrangements of electron and muon vacuum-polarization loops.

The result of numerical evaluation of (2.13), obtained by RIWIAD using 10^5 subcubes and 10 iterations, as well as the corresponding residual renormalization terms expressing the difference between the standard and K_S renormalizations, are listed in Table I. Numerical values of lower-order Feynman integrals, in terms of which the residual renormalization terms[25] are expressed, are given in Table II. From these tables we find

$$a[\text{Fig. 4(a)}] = 1.441\,6(18) , \quad (2.14)$$

$$a[\text{Fig. 4(b)}] = 0.172\,7(2) , \quad (2.15)$$

$$a[\text{Fig. 4(c)}] = 0.021\,6(1) . \quad (2.16)$$

Summing up (2.14)–(2.16), we find that the contribution of the subgroup I(c) to the muon anomaly is

$$a^{(8)}_{\mathrm{I(c)}} = 1.635\,9(19) . \quad (2.17)$$

The contribution to a_μ from the 15 diagrams of subgroup I(d) (see Fig. 5) can be written as

$$a_{2,P_{6i}} = \Delta M_{2,P_{6i}} + \text{residual renormalization terms} , \quad i = A,\ldots,H . \quad (2.18)$$

Divergence-free integrals $\Delta M_{2,P_{6i}}$ are defined by (4.13) of Ref. 22. They were evaluated numerically by RIWIAD with typically 3×10^5 subcubes and number of iterations ranging from 10 to 15, depending on the convergence rate. Their numerical values (multiplied by appropriate multiplicity factors η_i accounting for the diagrams related by time-reversal and charge-conjugation symmetries) are listed in the third column of Table I. The residual renormalization terms are listed in the fourth column of the same table.

Summing up the contributions of diagrams A–H of Fig. 5, we obtain

$$a^{(8)}_{\mathrm{I(d)}} = \sum_{i=A}^{H} \eta_i \Delta M_{2,P_{6i}} - 4\Delta B_2 \Delta M^{(\mu,e)}_{2,P_4} + 5(\Delta B_2)^2 M^{(\mu,e)}_{2,P_2} - 2(\Delta L^{(4)} + \Delta B^{(4)}) M^{(\mu,e)}_{2,P_2} - 2\Delta\delta m^{(4)} M^{(\mu,e)}_{2,P_2^*} , \quad (2.19)$$

TABLE I. Contributions of diagrams of Figs. 4 and 5 (η_i is the multiplicity factor).

Figure	η_i	$\eta_i\Delta M_i$	Residual renormalization terms
4(a)	1	1.580 3(18)	$-2\Delta B^{(e,e)}_{2,P_2} M^{(\mu,e)}_{2,P_2}$
4(b)	1	0.231 9(2)	$-2\Delta B^{(\mu,e)}_{2,P_2} M^{(\mu,\mu)}_{2,P_2}$
4(c)	1	0.021 6(1)	$-2\Delta B^{(e,\mu)}_{2,P_2} M^{(\mu,e)}_{2,P_2}$
5 A	2	5.411 4(74)	$-4\Delta' B_2 M^{(\mu,e)}_{2,P_{4b}} + 2(\Delta' B_2)^2 M^{(\mu,e)}_{2,P_2}$
5 B	1	2.900 2(63)	$-2\Delta' B_2 M^{(\mu,e)}_{2,P_{4b}} + (\Delta' B_2)^2 M^{(\mu,e)}_{2,P_2}$
5 C	2	1.365 5(33)	$-2\Delta' B_2 M^{(\mu,e)}_{2,P_{4b}} + 2(\Delta' B_2)^2 M^{(\mu,e)}_{2,P_2}$ $-2\Delta' B_{4b} M^{(\mu,e)}_{2,P_2} - 2\Delta\delta m_{4b} M^{(\mu,e)}_{2,P_2^*}$
5 D	2	−3.105 2(59)	$-4\Delta' L_2 \Delta M^{(\mu,e)}_{2,P_{4b}} + 4\Delta' L_2 \Delta' B_2 M^{(\mu,e)}_{2,P_2}$ $-2\Delta' B_{4a} M^{(\mu,e)}_{2,P_2} - 2\Delta\delta m_{4a} M^{(\mu,e)}_{2,P_2^*}$
5 E	4	−0.176 5(99)	$-4\Delta' L_2 \Delta M^{(\mu,e)}_{2,P_{4b}} + 8\Delta' L_2 \Delta' B_2 M^{(\mu,e)}_{2,P_2}$ $-4\Delta' L_{4s} M^{(\mu,e)}_{2,P_2} - 4\Delta' B_2 \Delta M^{(\mu,e)}_{2,P_{4a}}$
5 F	2	−4.037 7(71)	$+4(\Delta' L_2)^2 M^{(\mu,e)}_{2,P_2} - 4\Delta' L_{4c} M^{(\mu,e)}_{2,P_2}$ $-2\Delta' L_2 M^{(\mu,e)}_{2,P_{4a}}$
5 G	1	−0.208 4(86)	$+3(\Delta' L_2)^2 M^{(\mu,e)}_{2,P_2} - 2\Delta' L_{4i} M^{(\mu,e)}_{2,P_2}$ $-2\Delta' L_2 \Delta M^{(\mu,e)}_{2,P_{4a}}$
5 H	1	2.834 0(43)	$-2\Delta' L_{4x} M^{(\mu,e)}_{2,P_2}$

TABLE II. Auxiliary integrals—Group I. Column 3 lists relevant equations from Ref. 22. Note, however, that the treatment of terms related to the IR subtraction has been changed from that of Ref. 22 to that of Ref. 27. Thus, for instance, $\Delta B_{2,P_2}^{(e,e)}$ in this table corresponds to $\Delta B_{2,P_2}^{(e,e)}+\Delta L_{2,P_2}^{(e,e)}$ of Ref. 22.

Term	Value	Reference
$M_{2,P_2}^{(\mu,\mu)}$	0.015 687	(3.6)
$M_{2,P_2}^{(\mu,e)}$	1.094 259 6	(3.6)
$M_{2,P_2^*}^{(\mu,e)}$	−0.161 09(3)	(4.14)
ΔB_2	0.75	(4.15)
$\Delta B_{2,P_2}^{(e,e)}$	0.063 399	(4.7)
$\Delta B_{2,P_2}^{(\mu,e)}$	1.886 33(8)	(4.7)
$\Delta B_{2,P_2}^{(e,\mu)}$	$9.405\,5\times10^{-6}$	(4.7)
$\Delta M_{2,P_4}^{(\mu,e)}$	3.135 7(6)	(4.15)
$\Delta B_{4a}+2\Delta L_{4c}+\Delta L_{4x}$	−0.513 8(17)	(4.15)
$\Delta B_{4b}+2\Delta L_{4s}+\Delta L_{4l}$	0.542 4(6)	(4.15)
$\Delta\delta m_{4a}$	−0.301 5(10)	(4.15)
$\Delta\delta m_{4b}$	2.208 1(4)	(4.15)

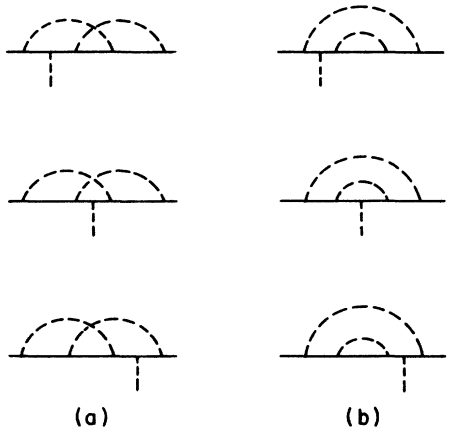

FIG. 6. (a) Fourth-order vertex diagrams with crossed photon lines. (b) Fourth-order vertex diagrams in which photon lines do not cross.

where

$$\eta_i=\begin{cases}1 & \text{for } i=B,G,H\ ,\\ 2 & \text{for } i=A,C,D,F\ ,\\ 4 & \text{for } i=E\ ,\end{cases} \tag{2.20}$$

and

$$\begin{aligned}&\Delta B_2=\Delta' B_2+\Delta' L_2=\tfrac{3}{4}\ ,\\ &\Delta M_{2,P_4}^{(\mu,e)}=\Delta M_{2,P_{4a}}^{(\mu,e)}+2\Delta M_{2,P_{4b}}^{(\mu,e)}\ ,\\ &\Delta L^{(4)}=\Delta L_{4x}+2\Delta L_{4c}+\Delta L_{4l}+2\Delta L_{4s}\ ,\\ &\Delta B^{(4)}=\Delta B_{4a}+\Delta B_{4b}\ ,\\ &\Delta\delta m^{(4)}=\Delta\delta m_{4a}+\Delta\delta m_{4b}\ .\end{aligned} \tag{2.21}$$

The quantities in (2.21) are defined[25] in Ref. 22. Their values are given in Table II. From the numerical values listed in Tables I and II we obtain

$$a_{\mathrm{I(d)}}^{(8)}=-0.794\,5(202)\ . \tag{2.22}$$

Finally, collecting the results (2.6), (2.11), (2.17), and (2.22), we find the contribution to the muon anomaly from the 49 diagrams of group I to be

$$a_{\mathrm{I}}^{(8)}=16.169(21)\ . \tag{2.23}$$

Group II

Diagrams of this group are generated by inserting second- and fourth-order vacuum-polarization loops in the photon lines of the fourth-order vertex diagrams in Figs. 6(a) and 6(b). Note that the diagrams of Fig. 6 can also be obtained from the fourth-order muon self-energy diagrams shown in Fig. 7 by inserting an external vertex in the open muon lines in all possible ways. Vertex diagrams derived from the same self-energy diagram share many properties and the corresponding Feynman integrals can be combined into a single compact integral with the help of the Ward-Takahashi identity, simplifying the computation substantially.

Use of the analytic expressions for the second- and fourth-order spectral functions for the photon propagator, the Ward-Takahashi identity, and time-reversal symmetry cuts down the number of independent integrals to be evaluated from 90 to 11.

The contribution to a_μ arising from the set of vertex diagrams represented by the self-energy diagram α ($=a$ though k'') of Fig. 8 can be written in the form

$$a_{4,P_\alpha}=\Delta M_{4,P_\alpha}+\text{residual renormalization terms}_\alpha\ , \tag{2.24}$$

where $\Delta M_{4,P_\alpha}$ are finite integrals obtained by trivially modifying those given by Eqs. (3.11), (3.17), and (3.22) of Ref. 26. Their numerical values, obtained by VEGAS using 10^7–4×10^7 subcubes and 30–40 iterations for each integral, are listed in Table III. The values of auxiliary integrals needed to calculate the total contribution of group II diagrams are given in Table IV. They were also evaluated by VEGAS using up to 10^7 subcubes and 30–40 iterations.

Summing contributions of diagrams $a-b''$, $c-f''$, and $g-k''$, respectively, we find

FIG. 7. Fourth-order muon self-energy diagrams containing no vacuum-polarization loops.

TABLE III. Contributions from various diagrams of Fig. 8. ($\eta_i = 1$ or 2 for symmetric and asymmetric diagrams respectively.)

Diagram	$\eta_i \Delta M_{4,P_i}$	Residual renormalization terms
$\Delta M^{(\mu,e)}_{4a,P_4}$	2.062 1(234)	$-2\Delta' L_2 M^{(\mu,e)}_{2,P_4} - 2\Delta' L^{(\mu,e)}_{2,P_4} M_2$
$\Delta M^{(\mu,e)}_{4b,P_{1':4}} + \Delta M^{(\mu,e)}_{4b,P_{0:4}}$	−6.178 1(97)	$-\Delta' B_2 M^{(\mu,e)}_{2,P_4} - \Delta' B^{(\mu,e)}_{2,P_4} M_2 + I_2 M^{(\mu,e)}_{2,P_4}$
$\Delta M^{(e,e)}_{4a,P_2,P_2}$	2.284 0(201)	$-2\Delta' L^{(\mu,e)}_{2,P_2} M^{(\mu,e)}_{2,P_2}$
$\Delta M^{(e,e)}_{4b,P_{1':2},P_{0:2}}$	−8.744 6(93)	$-\Delta' B^{(\mu,e)}_{2,P_2} M^{(\mu,e)}_{2,P_2}$
$\Delta M^{(e,\mu)}_{4a,P_2,P_2}$	0.053 7(47)	$-2\Delta' L^{(\mu,\mu)}_{2,P_2} M^{(\mu,e)}_{2,P_2} - 2\Delta' L^{(\mu,e)}_{2,P_2} M^{(\mu,\mu)}_{2,P_2}$
$\Delta M^{(e,\mu)}_{4b,P_{1':2},P_{0:2}}$	−0.285 5(5)	$-\Delta' B^{(\mu,\mu)}_{2,P_2} M^{(\mu,e)}_{2,P_2}$
$\Delta M^{(\mu,e)}_{4b,P_{1':2},P_{0:2}}$	−0.239 2(9)	$-\Delta' B^{(\mu,e)}_{2,P_2} M^{(\mu,\mu)}_{2,P_2}$
$\Delta M^{(e,e)}_{4a,P_{2:2}}$	5.186 9(270)	$-2\Delta' L_2 M^{(e,e)}_{2,P_{2:2}} - 2\Delta' L^{(e,e)}_{2,P_{2:2}} M_2$
$\Delta M^{(e,e)}_{4b,P_{1':2:2}} + \Delta M^{(e,e)}_{4b,P_{0:2:2}}$	−11.681 0(51)	$-\Delta' B_2 M^{(e,e)}_{2,P_{2:2}} - \Delta' B^{(e,e)}_{2,P_{2:2}} M_2 + I_2 M^{(e,e)}_{2,P_{2:2}}$
$\Delta M^{(e,\mu)}_{4a,P_{2:2}}$	0.261 7(4)	$-4\Delta' L_2 M^{(e,\mu)}_{2,P_{2:2}} - 4\Delta' L^{(e,e)}_{2,P_{2:2}} M_2$
$\Delta M^{(e,\mu)}_{4b,P_{1':2:2}} + \Delta M^{(e,\mu)}_{4b,P_{0:2;2}}$	−0.993 2(18)	$-2\Delta' B_2 M^{(e,\mu)}_{2,P_{2:2}} - 2\Delta' B^{(e,\mu)}_{2,P_{2:2}} M_2 + 2 I_2 M^{(e,\mu)}_{2,P_{2:2}}$

$$a_{4,P_4} = 2\Delta M^{(\mu,e)}_{4a,P_4} + \Delta M^{(\mu,e)}_{4b,P_{1':4}} + \Delta M^{(\mu,e)}_{4b,P_{0:4}} - \Delta B_2 M^{(\mu,e)}_{2,P_4} - \Delta B^{(\mu,e)}_{2,P_4} M_2 \ , \tag{2.25}$$

where $M^{(\mu,e)}_{2,P_4}$ is equal to $\Delta M^{(\mu,e)}_{2,P_4} - 2\Delta B_2 M^{(\mu,e)}_{2,P}$ [see (2.21)], and

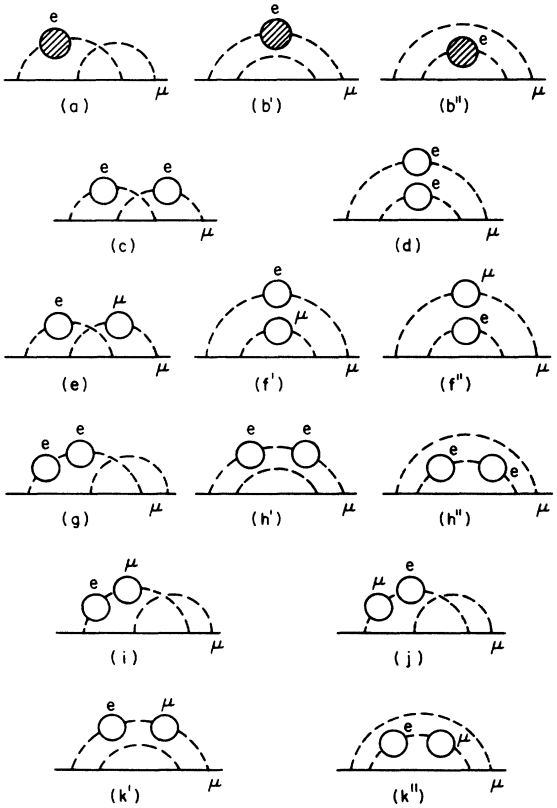

FIG. 8. Eighth-order muon self-energy diagrams obtained from the fourth-order diagrams of Fig. 7 by inserting vacuum-polarization loops. Seven more diagrams related to *a*, *e*, *g*, *i*, *j*, *k'*, and *k"* by time reversal are not shown. Shaded circles represent the sum of all fourth-order vacuum-polarization loops.

$$a_{4,P_2,P_2} = \Delta M^{(e,e)}_{4a,P_2,P_2} + \Delta M^{(e,e)}_{4b,P_{1':2},P_{0:2}} - \Delta B^{(\mu,e)}_{2,P_2} M^{(\mu,e)}_{2,P_2} + 2\Delta M^{(e,\mu)}_{4a,P_2,P_2} + \Delta M^{(e,\mu)}_{4b,P_{1':2},P_{0:2}} + \Delta M^{(\mu,e)}_{4b,P_{1':2},P_{0:2}} - \Delta B^{(\mu,\mu)}_{2,P_2} M^{(\mu,e)}_{2,P_2} - \Delta B^{(\mu,e)}_{2,P_2} M^{(\mu,\mu)}_{2,P_2} \ , \tag{2.26}$$

$$a_{4,P_{2:2}} = 2\Delta M^{(e,e)}_{4a,P_{2:2}} + \Delta M^{(e,e)}_{4b,P_{1':2:2}} + \Delta M^{(e,e)}_{4b,P_{0:2:2}} - \Delta B_2 M^{(e,e)}_{2,P_{2:2}} - \Delta B^{(e,e)}_{2,P_{2:2}} M_2 + 4\Delta M^{(e,\mu)}_{4a,P_{2:2}} + 2\Delta M^{(e,\mu)}_{4b,P_{1':2:2}} + 2\Delta M^{(e,\mu)}_{4b,P_{0:2:2}} - 2\Delta B_2 M^{(e,\mu)}_{2,P_{2:2}} - 2\Delta B^{(e,\mu)}_{2,P_{2:2}} M_2 \ . \tag{2.27}$$

TABLE IV. Auxiliary integrals—Group II. Column 3 lists relevant equations from Ref. 26. Note, however, that the treatment of terms related to IR subtraction has been changed from that of Ref. 26 to that of Ref. 27. Thus, equations quoted do not necessarily correspond exactly to the quantities listed. For instance, $\Delta B^{(\mu,e)}_{2,P_4}$ in this table is equal to $\Delta' B^{(\mu,e)}_{2,P_4} + \Delta' L^{(\mu,e)}_{2,P_4}$ in the notation of Ref. 26.

Term	Value	Reference
ΔB_2	0.75	(2.13)
$\Delta B^{(\mu,e)}_{2,P_4}$	2.440 8(11)	(3.12)
$\Delta B^{(\mu,e)}_{2,P_2}$	1.886 33(8)	(3.18)
$\Delta B^{(\mu,\mu)}_{2,P_2}$	0.063 399	(3.18)
$\Delta B^{(e,e)}_{2,P_{2:2}}$	5.331 9(15)	(3.23)
$\Delta B^{(e,\mu)}_{2,P_{2:2}}$	0.236 13(6)	(3.23)
M_2	0.5	(2.7)
$M^{(\mu,e)}_{2,P_4}$	1.494 3(6)	(3.4)
$M^{(\mu,e)}_{2,P_2}$	1.094 259 6	(3.16)
$M^{(\mu,\mu)}_{2,P_2}$	0.015 687	(3.16)
$M^{(e,e)}_{2,P_{2:2}}$	2.720 1(3)	(3.21)
$M^{(e,\mu)}_{2,P_{2:2}}$	0.050 28(1)	(3.21)

Note that the multiplicity factor for each term, which account for equivalent diagrams obtained by time reversal and/or interchange of electron and muon vacuum-polarization loops, is shown explicitly in the above formulas. Thus, entries in Table IV do not include multiplicity factors.

Substitution of the numerical values listed in Tables III and IV into (2.25)–(2.27) yields[25]

$$a_{4,P_4} = -2.786\,4(45) , \tag{2.28}$$

$$a_{4,P_2,P_2} = -4.558\,6(31) , \tag{2.29}$$

$$a_{4,P_{2:2}} = -9.357\,1(40) . \tag{2.30}$$

Combining these results the contribution to a_μ from the 90 diagrams of group II is found to be

$$a_{\rm II}^{(8)} = -16.702(7) . \tag{2.31}$$

Group III

These diagrams are generated by inserting a second-order vacuum-polarization loop into photon lines of muon vertex diagrams of three-photon-exchange type.

Time-reversal invariance, use of the function ρ_2 for the second-order photon spectral function [see (2.2)], summation over a set of proper vertex amplitudes that differ only in where the external magnetic field vertex is inserted, and transformation of these sums with the help of the Ward-Takahashi identity reduce the number of independent integrals to be evaluated from 150 to 8. These integrals have a one-to-one correspondence with the self-energy diagrams of Fig. 9 and can be written explicitly in terms of the parametric functions defined for the latter.

Let $M_{6\alpha,P}$ be the Ward-Takahashi-summed magnetic moment projection of the set of 15 vertex diagrams generated from a self-energy diagram α ($=A$ through H) of Fig. 9 by insertion of a second-order electron vacuum-polarization loop and an external vertex.[27] The renormalized contribution to a_μ due to the diagrams of group III can then be written as

$$a_{\rm III}^{(8)} = \sum_{\alpha=A}^{H} \eta_\alpha a_{6\alpha,P} , \tag{2.32}$$

where

$$a_{6\alpha,P} = \Delta M_{6\alpha,P} + \text{residual renormalization terms} ,$$

and

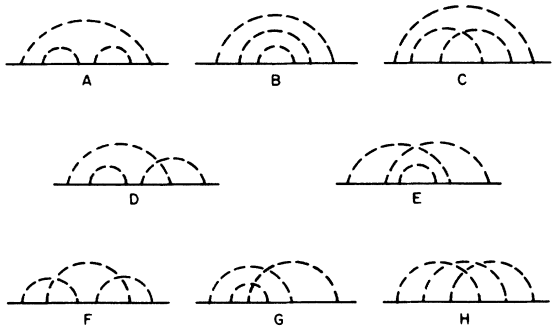

FIG. 9. Muon self-energy diagrams of the three-photon-exchange type. Two more diagrams related to D and G by time reversal are not shown.

$$\eta_\alpha = \begin{cases} 2 & \text{for } \alpha = D,G , \\ 1 & \text{for } \alpha = A,B,C,E,F,H , \end{cases} \tag{2.33}$$

which takes account of the time-reversed counterparts of the self-energy diagrams D and G of Fig. 9. $\Delta M_{6\alpha,P}$ is the UV- and IR-finite portion of $M_{6\alpha,P}$ where all divergences have been projected out by K_S and $I_{G/S}$ operations. Integrals $\Delta M_{6\alpha,P}$ ($\alpha = A$ through F and H) were evaluated by the integration routine VEGAS (Ref. 11) with 10^7 subcubes, the number of iterations ranging between 30 and 40 depending on the convergence rate of the integral.

The integral $\Delta M_{6G,P}$ required a special treatment because double precision arithmetic was not accurate enough to deal with the cancellation of UV divergences arising from a second-order vertex. This problem was resolved using quadruple precision arithmetic in a small region surrounding the singularity.[28] This region (1% of the whole domain) was sampled with 10^6 points per iteration while the rest was sampled in double precision with 10^7 points per iteration. The numbers of interactions were 34 and 37, respectively.

The latest results of a long sequence of numerical evaluation of group III integrals are summarized in the second column of Table V. The residual renormalization terms are shown in the third column of the same table. Numerical values of auxiliary integrals needed in the renormalization scheme are listed in Table VI.

When summed over all the diagrams of group III, the UV- and IR-divergent pieces cancel out and the total contribution to a_μ can be written as a sum of finite pieces:

$$\begin{aligned} a_{\rm III}^{(8)} = \sum_{\alpha=A}^{H} & \eta_\alpha \Delta M_{6\alpha,P} - 3\Delta B_{2,P}^{(\mu,e)}(\Delta M_{4a} + \Delta M_{4b}) - 3\Delta B_2(\Delta M_{4a,P}^{(\mu,e)} + \Delta M_{4b,P}^{(\mu,e)}) + M_{2^*,P}^{(\mu,e)}[I](\Delta\delta m_{4a} + \Delta\delta m_{4b}) \\ & + M_{2^*}[I](\Delta\delta m_{4a,P}^{(\mu,e)} + \Delta\delta m_{4b,P}^{(\mu,e)}) - M_{2^*,P}^{(\mu,e)}(\Delta\delta m_{4a} + \Delta\delta m_{4b}) - M_{2^*}(\Delta\delta m_{4a,P}^{(\mu,e)} + \Delta\delta m_{4b,P}^{(\mu,e)}) \\ & - M_{2,P}^{(\mu,e)}[B_{axc} + B_{bls} - 2(\Delta B_2)^2] - M_2(B_{axc,P}^{(\mu,e)} + B_{bls,P}^{(\mu,e)} - 4\Delta B_2 \Delta B_{2,P}^{(\mu,e)}) . \end{aligned} \tag{2.34}$$

Plugging in the values listed in Tables V and VI, we obtain[25]

$$a_{\rm III}^{(8)} = 10.793(48) . \tag{2.35}$$

As a byproduct of the calculation described above, one can also obtain the best numerical value available for the electron-loop vacuum-polarization contribution to the sixth-order a_μ, which can be written as

TABLE V. Contributions of grouped diagrams of Fig. 9. [$\eta_\alpha=1$ (2) for symmetric (asymmetric) diagrams.]

Diagram	$\eta_\alpha\Delta M_{6\alpha,P}$	Residual renormalization terms
A	−12.940 1(130)	$-2(\Delta' B_2\Delta M^{(\mu,e)}_{4b,P}+2\Delta' B^{(\mu,e)}_{2,P}\Delta M_{4b})+M^{(\mu,e)}_{2,P}(2I_{4s}+(\Delta' B_2)^2-2I_2\Delta' B_2)$ $+M_2(2I^{(\mu,e)}_{4s,P}+2\Delta' B_2\Delta' B^{(\mu,e)}_{2,P}-2I_2\Delta' B^{(\mu,e)}_{2,P}-2I^{(\mu,e)}_{2,P}\Delta' B_2)$
B	18.797 9(171)	$+\Delta M_{4b}(I^{(\mu,e)}_{2,P}-\Delta' B^{(\mu,e)}_{2,P})+\Delta M^{(\mu,e)}_{4b,P}(I_2-\Delta' B_2)$ $+\Delta\delta m_{4b}(M^{(\mu,e)}_{2^*,P}[I]-M^{(\mu,e)}_{2^*,P})+\Delta\delta m^{(\mu,e)}_{4b,P}(M_{2^*}[I]-M_{2^*})$ $+M^{(\mu,e)}_{2,P}(2I_{4s}+2I_{4l}-\Delta B_{4b}+(\Delta' B_2)^2+(I_2)^2-2\Delta' B_2 I_2)$ $+M_2(2I^{(\mu,e)}_{4s,P}+2I^{(\mu,e)}_{4l,P}-\Delta B^{(\mu,e)}_{4b,P}+2\Delta' B_2\Delta' B^{(\mu,e)}_{2,P}$ $+2I_2 I^{(\mu,e)}_{2,P}-2\Delta' B^{(\mu,e)}_{2,P}I_2-2\Delta' B_2 I^{(\mu,e)}_{2,P})$
C	4.000 7(178)	$+I^{(\mu,e)}_{2,P}\Delta M_{4a}+I_2\Delta M^{(\mu,e)}_{4a,P}-2I^{(\mu,e)}_{2,P}\Delta M_{4b}-2I_2\Delta M^{(\mu,e)}_{4b,P}$ $+\Delta\delta m^{(\mu,e)}_{4a,P}(M_{2^*}[I]-M_{2^*})+\Delta\delta m_{4a}(M^{(\mu,e)}_{2^*,P}[I]-M^{(\mu,e)}_{2^*,P})$ $+M^{(\mu,e)}_{2,P}[2I_{4c}+I_{4x}-\Delta B_{4a}-2(I_2)^2+2\Delta' B_2 I_2]$ $+M_2(2I^{(\mu,e)}_{4c,P}+I^{(\mu,e)}_{4x,P}-\Delta B^{(\mu,e)}_{4a,P}-4I_2 I^{(\mu,e)}_{2,P}+2\Delta' B^{(\mu,e)}_{2,P}I_2+2\Delta' B_2 I^{(\mu,e)}_{2,P})$
D	10.494 0(225)	$-\Delta' B^{(\mu,e)}_{2,P}\Delta M_{4a}-\Delta' B_2\Delta M^{(\mu,e)}_{4a,P}-I^{(\mu,e)}_{2,P}\Delta M_{4b}-I_2\Delta M^{(\mu,e)}_{4b,P}$ $+M^{(\mu,e)}_{2,P}[I_{4c}-I_{4s}-\Delta L_{4s}-(I_2)^2+2\Delta' B_2 I_2]$ $+M_2(I^{(\mu,e)}_{4c,P}-I^{(\mu,e)}_{4s,P}-\Delta L^{(\mu,e)}_{4s,P}-2I_2 I^{(\mu,e)}_{2,P}+2\Delta' B^{(\mu,e)}_{2,P}I_2+2\Delta' B_2 I^{(\mu,e)}_{2,P})$
E	11.000 1(121)	$-\Delta' B^{(\mu,e)}_{2,P}\Delta M_{4a}-\Delta' B_2\Delta M^{(\mu,e)}_{4a,P}+M^{(\mu,e)}_{2,P}(I_{4x}-2I_{4s}-2\Delta L_{4s}+2\Delta' B_2 I_2)$ $+M_2(I^{(\mu,e)}_{4x,P}-2I^{(\mu,e)}_{4s,P}-2\Delta L^{(\mu,e)}_{4s,P}+2\Delta' B^{(\mu,e)}_{2,P}I_2+2\Delta' B_2 I^{(\mu,e)}_{2,P})$
F	5.651 8(166)	$-2I^{(\mu,e)}_{2,P}\Delta M_{4a}-2I_2\Delta M^{(\mu,e)}_{4a,P}+M^{(\mu,e)}_{2,P}[-2I_{4c}-2\Delta L_{4c}+3(I_2)^2]$ $+M_2(-2I^{(\mu,e)}_{4c,P}-2\Delta L^{(\mu,e)}_{4c,P}+6I_2 I^{(\mu,e)}_{2,P})$
G	19.742 4(172)	$-I^{(\mu,e)}_{2,P}\Delta M_{4a}-I_2\Delta M^{(\mu,e)}_{4a,P}+M^{(\mu,e)}_{2,P}[-I_{4l}-I_{4c}-\Delta L_{4l}-\Delta L_{4c}+(I_2)^2]$ $+M_2(-I^{(\mu,e)}_{4l,P}-I^{(\mu,e)}_{4c,P}-\Delta L^{(\mu,e)}_{4l,P}-\Delta L^{(\mu,e)}_{4c,P}+2I_2 I^{(\mu,e)}_{2,P})$
H	−18.361 5(141)	$+M^{(\mu,e)}_{2,P}(-2I_{4x}-2\Delta L_{4x})+M_2(-2I^{(\mu,e)}_{4x,P}-2\Delta L^{(\mu,e)}_{4x,P})$

$$a_\mu^{(6)}(\text{vacuum polarization})$$
$$=\Delta M^{(\mu,e)}_{4a,P}+\Delta M^{(\mu,e)}_{4b,P}-\Delta B_2 M^{(\mu,e)}_{2,P}-\Delta B^{(\mu,e)}_{2,P}M_2$$
$$+M^{(\mu,e)}_{2,P4}+2M^{(e,\mu)}_{2,P_{2:2}}+M^{(e,e)}_{2,P_{2:2}}\ . \qquad (2.36)$$

TABLE VI. Auxiliary integrals—Group III.

Term	Value
$M_{2^*}[I]\Delta\delta m^{(\mu,e)}_{4b,P}+M^{(\mu,e)}_{2^*,P}[I]\Delta\delta m_{4b}$	−15.501 8(16)
$M_{2^*}[I]\Delta\delta m^{(\mu,e)}_{4a,P}+M^{(\mu,e)}_{2^*,P}[I]\Delta\delta m_{4a}$	0.185 7(25)
M_2	0.5
$M^{(\mu,e)}_{2,P}$	1.094 259 6
M_{2^*}	1.0
$M^{(\mu,e)}_{2^*,P}$	2.350 8(8)
ΔB_2	0.75
$\Delta B^{(\mu,e)}_{2,P}$	1.886 33(8)
$\Delta\delta m_{4a}$	−0.301 5(10)
$\Delta\delta m^{(\mu,e)}_{4a,P}$	0.472 9(12)
$\Delta\delta m_{4b}$	2.208 1(4)
$\Delta\delta m^{(\mu,e)}_{4b,P}$	10.678 6(12)
ΔM_{4a}	0.218 3
$\Delta M^{(\mu,e)}_{4a,P}$	1.728 7(10)
ΔM_{4b}	−0.187 5
$\Delta M^{(\mu,e)}_{4b,P}$	−2.359 8(6)
B_{axc}	−0.987 3(26)
$B^{(\mu,e)}_{axc,P}$	−6.195 8(17)
B_{bls}	1.482 3(9)
$B^{(\mu,e)}_{bls,P}$	9.009 3(15)

Substituting the data from Tables IV and VI in (2.36) we obtain the value given in (1.7).

Group IV

Diagrams of this group can be divided into four subgroups. Each subgroup consists of two equivalent sets of diagrams related by charge conjugation (reversal of the direction of momentum flow in the loop of the light-by-light scattering subdiagram).

Subgroup IV(a). Diagrams obtained by inserting a second-order vacuum-polarization loop in the sixth-order light-by-light scattering diagrams. This subgroup is comprised of 54 diagrams. A typical diagram is shown in Fig. 10(a). Use of the Ward-Takahashi identity to sum over external vertex insertions, summation over second-order vacuum-polarization-loop insertions, and charge-conjugation symmetry reduce to just three the number of independent integrals to be evaluated. They are all appropriate modifications of the integral $M_{6LL,P}$ defined by (2.4) of Ref. 29. Denote these integrals by $M^{(l_1,l_2)}_{6LL,P}$ where $(l_1,l_2)=(e,e)$, (e,μ), or (μ,e). They are generically represented by the self-energy diagrams shown in Fig. 11.

Subgroup IV(b). Diagrams containing sixth-order light-by-light scattering subdiagram. Altogether, there are 60 diagrams of this type. An example is shown in Fig. 10(b). Charge-conjugation and time-reversal symmetries and summation over external vertex insertions reduce to four the number of integrals to be evaluated. These integrals are generically represented by the self-

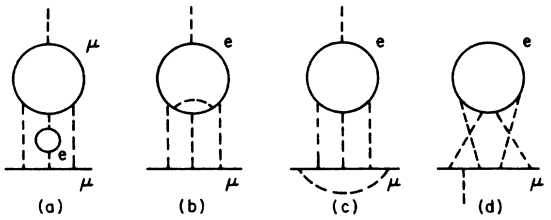

FIG. 10. Representative diagrams of each subgroup of group IV.

energy diagrams *LL A*, *LLB*, *LLC*, and *LLD* of Fig. 12.

Subgroup IV(c). Diagrams obtained by attaching a single virtual-photon line to the muon line of the sixth-order vertex containing a fourth-order electron-loop light-by-light scattering diagram. There are 48 diagrams that belong to this subgroup. An example is shown in Fig. 10(c). Summation over external vertex insertions and use of the interrelations available due to charge-conjugation and time-reversal symmetries leave five independent integrals to be evaluated. They are generically represented by the self-energy diagrams *LLE*, *LLF*, *LLG*, *LLH*, and *LLI* of Fig. 12.

Subgroup IV(d). Diagrams generated by inserting a fourth-order light-by-light scattering subdiagram internally in a fourth-order vertex diagram. An example is shown in Fig. 10(d). Diagrams of this kind appear for the first time in the eighth order. Charge-conjugation invariance and summation over the external vertex insertion with the help of the Ward-Takahashi identity leads us to three independent integrals. They are represented by the diagrams *LLJ*, *LLK*, and *LLL* of Fig. 12.

The renormalized contribution to the muon anomaly arising from group IV diagrams can be written in the standard renormalization scheme as

$$a_{\mathrm{IV}}^{(8)}=a_{\mathrm{IV(a)}}^{(8)}+a_{\mathrm{IV(b)}}^{(8)}+a_{\mathrm{IV(c)}}^{(8)}+a_{\mathrm{IV(d)}}^{(8)}$$
$$=\sum_{(l_1,l_2)} a_{6LL,P}^{(l_1,l_2)}+\sum_{\alpha=A}^{L}\eta_\alpha a_{8LL\alpha}\ , \tag{2.37}$$

where

$$a_{6LL,P}^{(l_1,l_2)}=M_{6LL,P}^{(l_1,l_2)}+\text{renormalization terms}\ , \tag{2.38}$$

$$a_{8LL\alpha}=M_{8LL\alpha}+\text{renormalization terms}\ , \tag{2.39}$$

and

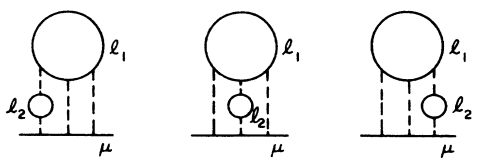

FIG. 11. Self-energy diagrams representing the external-vertex-summed integrals of subgroup IV(a).

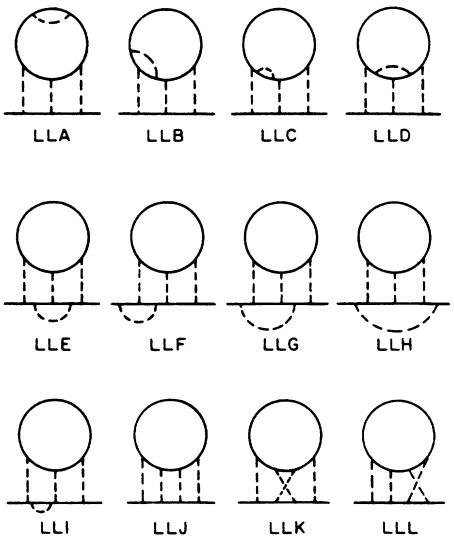

FIG. 12. Self-energy diagrams representing the external-vertex-summed integrals of subgroups IV(b), IV(c), and IV(d).

$$\eta_\alpha=\begin{cases}2 & \text{for } \alpha=B,C,F,G,I\ ,\\ 1 & \text{for } \alpha=A,D,E,H,J,K,L\ ,\end{cases} \tag{2.40}$$

accounts for diagrams related by time reversal. The factor 2 coming from equivalent diagrams obtained by reversing the momentum flow in the electron loop is included in the definitions (2.38) and (2.39).

For subgroups (a), (b), and (c), the UV divergence arising from the light-by-light scattering subdiagram $\Pi^{\nu\alpha\beta\gamma}(q,k_i,k_j,k_l)$ are taken care of by making use of the identity

$$\Pi^{\nu\alpha\beta\gamma}(q,k_i,k_j,k_l)=-q_\mu\left[\frac{\partial}{\partial q_\nu}\Pi^{\mu\alpha\beta\gamma}(q,k_i,k_j,k_l)\right]\ , \tag{2.41}$$

which follows from the Ward-Takahashi identity and the fact that self-energy diagrams to which vertex diagrams of these subgroups are related vanish by Furry's theorem. On the other hand, the self-energy diagrams from which diagrams of subgroup (d) are derived are nonzero and the UV divergence associated with the light-by-light scattering subdiagram must be regularized in the manner of Pauli and Villars. For these diagrams it is necessary to carry out explicit renormalizations of the light-by-light subdiagram as well as two sixth-order vertex subdiagrams which contain it. For details see Ref. 29.

Making use of (2.41) and the second-order photon spectral function, one finds that integrals $M_{6LL,P}^{(l_1,l_2)}$ are all finite, implying

$$a_{6LL,P}^{(l_1,l_2)}=M_{6LL,P}^{(l_1,l_2)}\equiv\Delta M_{6LL,P}^{(l_1,l_2)}\ , \tag{2.42}$$

so that the contribution of subgroup IV(a) is given by

$$a_{\mathrm{IV(a)}}^{(8)}=\sum_{(l_1,l_2)}\Delta M_{6LL,P}^{(l_1,l_2)}\ . \tag{2.43}$$

Relating the IR- and UV-divergent $M_{8LL\alpha}$ to the finite, numerically calculable piece $\Delta M_{8LL\alpha}$ defined by the procedure of intermediate renormalization of Ref. 29, one can write (2.39) in the form

$$a_{8LL\alpha}=\Delta M_{8LL\alpha}+\text{residual renormalization terms} . \tag{2.44}$$

Specifically, the contributions of the diagrams of subgroups (b) and (c) are given by

$$a^{(8)}_{\mathrm{IV(b)}}=\sum_{\alpha=A}^{D}\eta_\alpha\Delta M_{8LL\alpha}-3\Delta B_2 M_{6LL} , \tag{2.45}$$

and

$$a^{(8)}_{\mathrm{IV(c)}}=\sum_{\alpha=E}^{I}\eta_\alpha\Delta M_{8LL\alpha}-2\Delta B_2 M_{6LL} . \tag{2.46}$$

M_{6LL} appearing in (2.45) and (2.46), which is identical with the second quantity in (1.7), is the contribution to the muon anomaly from the sixth-order vertex diagrams containing an electron-loop light-by-light scattering subdiagram. On the other hand, the contribution of the subgroup (d) is written as

$$a^{(8)}_{\mathrm{IV(d)}}=\sum_{\alpha=J}^{L}\eta_\alpha a_{8LL\alpha} , \tag{2.47}$$

where $a_{8LL\alpha}$ is obtained by the standard renormalization instead of the intermediate renormalization (see Ref. 29).

Summing (2.43)–(2.47), we arrive at

$$a^{(8)}_{\mathrm{IV}}=\sum_{(l_1,l_2)}\Delta M^{(l_1,l_2)}_{6LL,P}+\sum_{\alpha=A}^{I}\eta_\alpha\Delta M_{8LL\alpha} -5\Delta B_2 M_{6LL}+\sum_{\alpha=J}^{L}\eta_\alpha a_{8LL\alpha} . \tag{2.48}$$

TABLE VII. Numerical results for various terms in (2.48). [$\eta_\alpha=1$ (2) for symmetric (asymmetric) diagrams.]

Diagram	$\eta_\alpha\Delta M_{8LL\alpha}$
$M^{(e,e)}_{6LL,P}$	116.805 1(609)
$M^{(e,\mu)}_{6LL,P}$	2.701 5(44)
$M^{(\mu,e)}_{6LL,P}$	4.325 7(130)
A	49.882 0(872)
B	−74.485 8(1048)
C	102.370 1(1248)
D	−37.810 6(1024)
E	−21.547 5(688)
F	−75.402 5(2031)
G	−34.942 1(1374)
H	54.091 3(1564)
I	112.662 9(1519)
J	5.457 5(206)
K	−7.828 9(340)
L	−1.067 3(355)
ΔB_2	0.75
M_{6LL}	20.947 1(29)

Numerical integration of all terms in (2.48) has been carried out using VEGAS (Ref. 11). The latest results are listed in Table VII. The number of iterations employed in achieving the stated results was between 25 and 40, while the number of function calls per iteration ranged from 4×10^6 to 12×10^6. In general, the major difficulty in dealing with the diagrams of this group arises from the enormous size of the integrands (up to 5000 terms and 240 kilobytes of FORTRAN source code per integral) and the large number of integration variables (up to 10). See Ref. 29 for a discussion of various computational problems encountered in the numerical integration.

Collecting the results of Table VII, we find the contribution from all 180 diagrams of group IV to be

$$a^{(8)}_{\mathrm{IV}}=116.660(405) . \tag{2.49}$$

Finally, combining (2.23) with (2.31), (2.35), and (2.49), we obtain the complete eighth-order QED contribution $A_2^{(8)}(m_\mu/m_e)$ reported in (1.9).

III. AN ESTIMATE OF THE TENTH-ORDER TERM

In view of the large eighth-order coefficient (1.9), one may naturally wonder how large the tenth-order coefficient might be. To answer this question unambiguously, one has to evaluate all tenth-order terms, a formidable task indeed. To achieve our goal of determining a_μ to a precision of few parts in 10^{-11}, however, it is sufficient if a rough but fairly reliable estimate is available.

Fortunately, it is not difficult to obtain such an estimate. It is based on the following empirical facts accumulated while working on the sixth- and eighth-order terms.

(a) The contribution of a minimal (gauge-invariant) set of diagrams is of order 1 as far as they have no closed electron loop. We mean by "minimal" a gauge-invariant set whose subsets (excluding itself) are not gauge invariant.

(b) The contribution of a minimal set of diagrams containing n electron vacuum-polarization loops is of order $[\ln(m_\mu/m_e)]^n$ times the term obtained by omitting these loops. In addition, it has a multiplicative factor which depends on the number of ways electron loop insertions can be made.

(c) The contribution of a minimal set of diagrams containing an electron loop light-by-light scattering subdiagram has a $\ln(m_\mu/m_e)$ factor with a large numerical coefficient. If it also contains electron vacuum-polarization loops, it is multiplied by further $\ln(m_\mu/m_e)$ factors.

Summing over a gauge-invariant set is a necessity since an individual diagram is UV and/or IR divergent in general. As examples of minimal sets, let us list the contributions of subgroups IV(b) and IV(c):

$$a^{(8)}_{\mathrm{IV(b)}}=-7.175(212),\quad a^{(8)}_{\mathrm{IV(c)}}=3.441(336) . \tag{3.1}$$

As is seen from Table VII, even the convergent parts of individual terms of these subgroups, which are not gauge invariant, may be very large, but their gauge-invariant

sums are fractions of M_{6LL} in (2.45), or its equivalent in (1.7).

One may conclude from this that the most important tenth-order term comes from 36 Feynman diagrams of the type shown in Figs. 13(a) and 13(b), which contain one light-by-light electron loop and two second-order electron vacuum-polarization loops. It is not difficult to write down a FORTRAN program for the sum of all these diagrams, adapting Eqs. (3.13) and (3.19) of Ref. 26 to this case. We evaluated this integral numerically. Our result, based on 28 iterations with 10^7 function calls per iteration, is

$$A_2^{(10)}(m_\mu/m_e;\ \text{leading term})=569.33(61)\ . \tag{3.2}$$

Of course, direct evaluation of other terms is much more tedious. Instead, we shall just give a rough estimate based on the observation that the effect of second-order electron loop insertion can be estimated as follows.[30] First note that such an insertion results in a modification of the photon propagator of the form (A10). Asymptotically we find

$$d_R^\infty\left[\frac{q^2}{m_e^2},\alpha\right]=1+\frac{\alpha}{\pi}\left[\tfrac{1}{3}\ln(q^2/m_e^2)-\tfrac{5}{9}\right]+\cdots\ , \qquad q^2\gg m_e^2\ . \tag{3.3}$$

Since the logarithm is a slowly varying function of q^2, one may replace q^2 by an average value $r^2m_\mu^2$, where r is a constant of order unity. This means that the insertion of a vacuum-polarization loop can be effectively reduced to multiplication by a factor

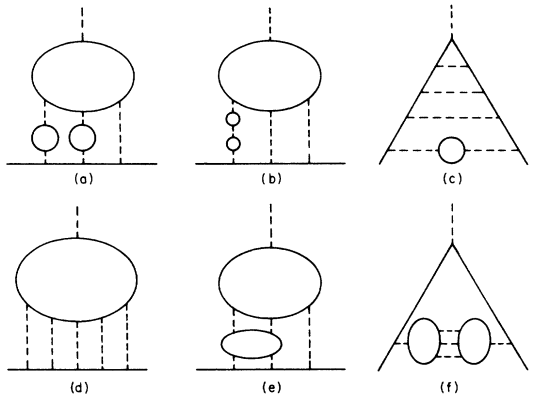

FIG. 13. Some tenth-order diagrams. (a) and (b) are generated by inserting two electron vacuum-polarization loops in a sixth-order diagram containing a light-by-light scattering subdiagram. There are 36 diagrams of these types. (c) is generated by inserting an electron vacuum-polarization loop in an electron-loop-free eighth-order diagram. There are 2072 diagrams belonging to this group. (d) contains a six-point electron loop. This group appears for the first time in the tenth order and consists of 120 diagrams. (e) and (f) contain two light-by-light scattering subdiagrams.

$$\frac{\alpha}{\pi}K=\frac{\alpha}{\pi}\left[\tfrac{2}{3}\ln(rm_\mu/m_e)-\tfrac{5}{9}\right]\ . \tag{3.4}$$

In order that the approximation (3.4) makes sense, r should be less than ~ 1 which means that K should be less than ~ 3.

Let us now estimate the magnitude of K from the previously calculated results. For example, for the eighth-order diagrams $M_{6LL,P}^{(e,e)}$ of Fig. 11 we will have

$$M_{6LL,P}^{(e,e)}\sim 3KA_2^{(6)}(m_\mu/m_e;\ \text{light-by-light})\ . \tag{3.5}$$

The factor 3 accounts for the number of photon lines in which an electron vacuum-polarization loop can be inserted. Similarly we may fix the parameter K from the relation

$$A_2^{(10)}(m_\mu/m_e;\ \text{leading term})\sim 6K^2A_2^{(6)}(m_\mu/m_e;\ \text{light-by-light})\ . \tag{3.6}$$

The factor 6 arises because two electron vacuum-polarization loops can be inserted in three photon lines in six different ways. Using the data from Table VII, and Eqs. (1.7) and (3.2), we find $K=1.86$ and 2.13 from (3.5) and (3.6), respectively. Examination of other diagrams yields K mostly in the range from 2 to 2.5 with the exception of $a_{\rm III}^{(8)}$ of (2.35) which gives $K\sim 4$. For our purpose it is sufficient to choose

$$K=2\sim 4\ . \tag{3.7}$$

This shows how poor the approximation (3.4) might actually be. What is most important, however, is that these K's are all positive. This means that one can confidently predict the signs of terms obtained by insertion of vacuum-polarization loops.

It is not difficult to turn this heuristic argument into a more rigorous one using the renormalization-group technique discussed in the Appendix. However, it will not be necessary for our present purpose.

As an application of the admittedly very crude method described above, let us estimate the magnitude of the term representing the sum of 2072 Feynman diagrams of the type shown in Fig. 13(c), which are obtained from 518 electron-loop-free eighth-order diagrams by insertion of an electron vacuum-polarization loop in all possible manners. Our estimate for this term is

$$4\times K\times(-1.98)=-(16-32)\ , \tag{3.8}$$

where 4 is the number of virtual photons and the factor -1.98 is from Ref. 16.

Similar estimate can be made for each minimal gauge-invariant subgroup discussed in Sec. II. In view of the fact that the results (2.23), (2.31), (2.35), as well as (3.1) and other gauge-invariant results calculable from Table VII, are no larger than 17 in magnitude and tend to cancel each other, one finds that the contribution of tenth-order diagrams obtained by insertion of a second-order vacuum-polarization loop in all eighth-order diagrams, excluding the result (3.2), is likely to be substantially less than 100.

Tenth-order diagrams that cannot be estimated by the method discussed above are of the types shown in Figs.

13(d)–13(f). Since they have low powers of $\ln(m_\mu/m_e)$, however, it seems to be unlikely that they give large contributions. In view of the fact that we do not know why the sixth-order diagrams containing a light-by-light scattering subdiagram have such a large value, however, it might not be prudent to rule out a surprise in the tenth order. Direct evaluation of contributions of Figs. 13(d)–13(f) might be interesting.

Our conservative estimate, then, is that the tenth-order term will be found well within the range given by

$$A_2^{(10)} = 570(140) . \tag{3.9}$$

This amounts to $39(10)\times 10^{-12}$ in the final value (1.17) for $a_\mu^{\rm QED}$.

ACKNOWLEDGMENTS

We thank R. F. Peierls, H. Sugawara, and H. Miyazawa for their encouragement and support at various phases of this work. Support by the computing centers of the Brookhaven National Laboratory, the National Laboratory for High Energy Physics (KEK), Japan, and Tokyo University, where parts of the computation were carried out, is gratefully acknowledged. The last phase of this research was conducted at the Cornell National Supercomputer Facility, a resource of the Center for Theory and Simulation in Science and Engineering (Theory Center), which receives major funding from the National Science Foundation and the IBM Corporation, with additional support from New York State and members of the Corporate Research Institute. The results reported here are based on about 200 hours of vectorized computation on the HITAC *S*-810 at KEK and more than 2000 hours in the scalar mode on the IBM-3090 at the Cornell National Supercomputing Facility. Note that one hour on an *S*-810 corresponds to about 30 hours on an IBM-3090. This work was supported, in part, by the National Science Foundation.

APPENDIX: COMPARISON WITH THE RENORMALIZATION-GROUP RESULTS

Because of the large mass ratio, $m_\mu/m_e \approx 207$, the leading contribution to the muon anomaly arising from the electron vacuum-polarization insertion is governed by the short-distance behavior of the photon propagator. Exploiting the relationship of this fact and the renormalization procedure it is possible to predict the $\ln(m_\mu/m_e)$ structure for a large number of diagrams contributing to a_μ (Ref. 30). Refining this technique further, Lautrup and de Rafael[31] were able to predict the complete $\ln(m_\mu/m_e)$ structure of a large class of eighth-order diagrams contributing to a_μ. The purpose of this appendix is to compare the numerical results obtained in Sec. II with the corresponding formulas derived in Ref. 31 and determine as much as possible the terms that were left undetermined by the latter. In order to make this paper somewhat self-containing, we start with a brief review of their methods and results.

Let us denote by $a(m_\mu/m_e,\alpha)$ the contribution to the muon anomaly from the class of vertex diagrams which are obtained by replacing all internal photon lines in a certain set of renormalized muon vertices by dressed renormalized photon propagators whose fermion loops are exclusively of the electron type. (See Fig. 14.) The starting set of muon vertices may contain muon loops to which any number of photon lines are attached. It may even include electron loops to which four or more photon lines are attached. For simplicity, however, let us first consider the case where the starting set is the largest set containing all types of muon loops but no electron loop at all. Actually, for some smaller starting sets, it is possible to extract more information. Some of them will be considered later.

According to the procedure of Ref. 31, we define its asymptotic part, $a_\infty(m_\mu/m_e,\alpha)$, as follows. In each order of perturbation theory drop terms which vanish as $m_\mu/m_e \to \infty$, while retaining terms which are constant or increase logarithmically. It can be shown that a_∞ obeys the homogeneous Callan-Symanzik equation

$$\left[m_e\frac{\partial}{\partial m_e}+\beta(\alpha)\alpha\frac{\partial}{\partial\alpha}\right]a_\infty\left[\frac{m_\mu}{m_e},\alpha\right]=0 . \tag{A1}$$

The solution to this equation is

$$\begin{aligned} a_\infty\left[\frac{m_\mu}{m_e},\alpha\right] &= \left[\frac{m_\mu}{m_e}\right]^{\beta(\alpha)\alpha(\partial/\partial\alpha)} B(\alpha) \\ &= \sum_{n=0}^{\infty}\frac{1}{n!}\left[\ln\frac{m_\mu}{m_e}\right]^n\left[\beta(\alpha)\alpha\frac{\partial}{\partial\alpha}\right]^n B(\alpha) , \end{aligned} \tag{A2}$$

where $\beta(\alpha)$ is the Callan-Symanzik function and

$$B(\alpha)=a_\infty\left[\frac{m_\mu}{m_e},\alpha\right]_{m_\mu=m_e}$$

is the nonlogarithmic part of a_∞. As is seen from Eq. (A2), knowledge of $\beta(\alpha)$ and $B(\alpha)$ determines a_∞ completely. Expanding $\beta(\alpha)$ and $B(\alpha)$ in powers of α/π as

$$\beta(\alpha)=\sum_{k=1}^{\infty}\beta_k\left[\frac{\alpha}{\pi}\right]^k , \quad B(\alpha)=\sum_{k=1}^{\infty}B_k\left[\frac{\alpha}{\pi}\right]^k ,$$

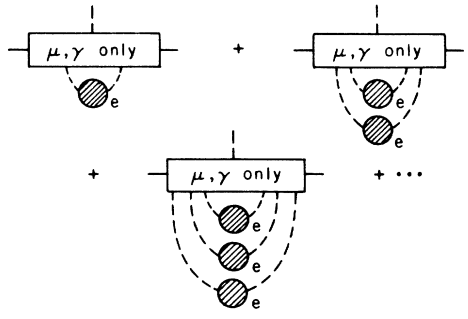

FIG. 14. A class of diagrams generated by inserting electron vacuum-polarization loops into a muon vertex.

and substituting them into Eq. (A2), we can determine the terms $a_\infty^{(n)}$, $n=2,4,6,\ldots$, successively. We are particularly interested in the eighth-order contribution $a_\infty^{(8)}(m_\mu/m_e,\alpha)$ which can be written in the form

$$a_\infty^{(8)}\left[\frac{m_\mu}{m_e},\alpha\right]=\left[\frac{\alpha}{\pi}\right]^4\left[B_4+C_4\ln\frac{m_\mu}{m_e}+D_4\ln^2\frac{m_\mu}{m_e}+E_4\ln^3\frac{m_\mu}{m_e}\right], \tag{A3}$$

where

$$C_4=\beta_3B_1+2\beta_2B_2+3\beta_1B_3\ ,\qquad D_4=\tfrac{5}{2}\beta_1\beta_2B_1+3\beta_1^2B_2,\quad E_4=\beta_1^3B_1\ . \tag{A4}$$

The functions $\beta(\alpha)$ and $B(\alpha)$ are both known up to the sixth order in perturbation theory. The coefficients β_k ($k=1,2,3$) are given by[32]

$$\beta_1=\tfrac{2}{3},\quad \beta_2=\tfrac{1}{2},\quad \beta_3=-\tfrac{121}{144}\ , \tag{A5}$$

while the values of B_k ($k=1,2,3$) are[16,30,33]

$$B_1=\tfrac{1}{2},\quad B_2=-1.022\,923\ldots,\quad B_3=2.741\,64(56)\ . \tag{A6}$$

Substituting (A4)–(A6) in (A3) one obtains

$$a_\infty^{(8)}\left[\frac{m_\mu}{m_e},\alpha\right]=\left[\frac{\alpha}{\pi}\right]^4[B_4+17.067\,6(60)]\ . \tag{A7}$$

Of the 469 eighth-order Feynman diagrams that contribute to $A_2^{(8)}(m_\mu/m_e)$, 304 belong to the class represented schematically by the diagrams shown in Fig. 14. It is the contribution of these diagrams to a_∞ that is given by (A7). These 304 diagrams consist of (i) all diagrams of group I with the exception of those shown in Fig. 4(c), (ii) all diagrams of group II, (iii) all diagrams of group III, (iv) diagrams of group IV which are represented by the self-energy diagrams of Fig. 11 with $(l_1,l_2)=(\mu,e)$. Having evaluated the contribution to the muon anomaly from these 304 diagrams "exactly," we are now in a position to extract the value of the previously undetermined coefficient B_4. Summing the results (2.6), (2.11), (2.14), (2.15), (2.22), (2.31), (2.35), and $M_{6LL,P}^{(\mu,e)}$ (third entry in Table VII), we find

$$a^{(8)}\left[\frac{m_\mu}{m_e},\alpha\right]=14.565(55)\left[\frac{\alpha}{\pi}\right]^4, \tag{A8}$$

which, when compared with (A7), means that

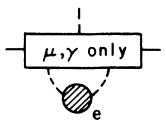

FIG. 15. A class of diagrams generated by inserting electron vacuum-polarization loops into a single photon line of an arbitrary muon vertex.

$$B_4=-2.503(55)+O\left[\frac{m_e}{m_\mu}\ln\frac{m_\mu}{m_e}\right]. \tag{A9}$$

The method used above was such that, because of lumping together of all the diagrams at a given order, information about individual diagrams was lost. Also, for the eighth-order calculation, it was possible to determine only the logarithmic mass dependence of $a_\infty^{(8)}$. The mass-independent term B_4 in (A3) could not be determined until direct evaluation (A8) was made. There is, however, a class of eighth-order diagrams whose contributions to $a_\infty^{(8)}$, including mass-independent terms in some cases, can be obtained by making use of the asymptotic form of the vacuum-polarization and lower-order anomalies. Diagrams which belong to this class are those that are generated by inserting an electron vacuum-polarization loop into a single photon line of an arbitrary muon vertex. (See Fig. 15.) In order to consider the contributions of this class of diagrams we start with a brief discussion of the asymptotic photon propagator.

The general expression for the renormalized photon propagator is of the form

$$D_R^{\mu\nu}(q)=-i\frac{g^{\mu\nu}}{q^2}d_R\left[\frac{q^2}{m_e^2},\alpha\right]+\text{the } q_\mu q_\nu \text{ term}\ . \tag{A10}$$

The asymptotic part of the renormalized photon propagator is defined as follows. In each order of perturbation theory drop terms that vanish in the limit $-q^2/m_e^2\to\infty$ while keeping divergent and constant terms. The asymptotic propagator satisfies the following Callan-Symanzik equation:[34]

$$\left[m_e\frac{\partial}{\partial m_e}+\beta(\alpha)\alpha\frac{\partial}{\partial\alpha}\right]\alpha d_R^\infty\left[-\frac{q^2}{m_e^2},\alpha\right]=0\ . \tag{A11}$$

The solution of this equation may be expanded in the form

$$d_R^\infty\left[-\frac{q^2}{m_e^2},\alpha\right]=1-(a_1+b_1L)\left[\frac{\alpha}{\pi}\right]+[-(a_2+b_2L)+(a_1+b_1L)^2]\left[\frac{\alpha}{\pi}\right]^2+[-(a_3+b_3L+c_3L^2)+2(a_1+b_1L)(a_2+b_2L)-(a_1+b_1L)^3]\left[\frac{\alpha}{\pi}\right]^3+\cdots, \tag{A12}$$

where

$$L=\ln\left[-\frac{q^2}{m_e^2}\right]. \tag{A13}$$

The first few coefficients are known from perturbation theory:[31]

$$b_1=-\tfrac{1}{3},\quad a_1=\tfrac{5}{9},\quad b_2=-\tfrac{1}{4},\quad a_2=\tfrac{5}{24}-\zeta(3)\ ,\qquad c_3=-\tfrac{1}{24},\quad b_3=\tfrac{47}{96}-\tfrac{1}{3}\zeta(3)\ . \tag{A14}$$

The coefficient a_3 has not been determined thus far. We are now ready to evaluate it.

From (A12) one can clearly see which contributions come from proper vacuum-polarization diagrams, which come from improper diagrams consisting of two proper parts, and which come from improper diagrams consisting of three proper diagrams, etc. Having found the asymptotic form of the photon propagator, we now turn to the discussion of the contribution to a_∞ from the diagrams that belong to the class represented by the diagram shown in Fig. 15.

We start by considering the diagrams shown in Fig. 16, generated by inserting the electron vacuum-polarization diagram G into the lowest-order muon vertex. An exact expression for the contribution to the muon anomaly from these diagrams is given by[31]

$$a_{(2;G)}=\frac{\alpha}{\pi}\int_0^1 dx(1-x)\left[d_R\left[\frac{-x^2}{1-x}\frac{m_\mu^2}{m_e^2}\right]-1\right]_{(G)}. \quad \text{(A15)}$$

Since we are interested in the asymptotic contribution to the anomaly, we have

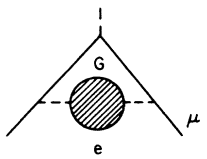

FIG. 16. Diagrams obtained by inserting electron vacuum-polarization loops into the second-order muon vertex.

$$a^\infty_{(2;G)}=\frac{\alpha}{\pi}\int_0^1 dx(1-x)\left[d_R^\infty\left[\frac{-x^2}{1-x}\frac{m_\mu^2}{m_e^2}\right]-1\right]_{(G)}. \quad \text{(A16)}$$

Eighth-order diagrams that belong to the class represented in Fig. 16 are those shown in Figs. 2(a), 3(a), 4(a), and 5. From (A12)–(A14) and (A16) one finds[31]

$$a^\infty_{(2;2:2:2)}=a^\infty[\text{Fig. 2(a)}]$$
$$=\left[-\tfrac{8609}{5832}-\tfrac{25}{162}\pi^2-\tfrac{2}{9}\zeta(3)+(\tfrac{317}{162}+\tfrac{2}{27}\pi^2)\ln\frac{m_\mu}{m_e}-\tfrac{25}{27}\ln^2\frac{m_\mu}{m_e}+\tfrac{4}{27}\ln^3\frac{m_\mu}{m_e}\right]\left[\frac{\alpha}{\pi}\right]^4$$
$$=7.1967\left[\frac{\alpha}{\pi}\right]^4, \quad \text{(A17)}$$

$$a^\infty_{(2;2:4)}=a^\infty[\text{Fig. 3(a)}]$$
$$=\left[\tfrac{509}{432}+\frac{\pi^2}{18}-\tfrac{25}{18}\zeta(3)+[-\tfrac{5}{4}+\tfrac{2}{3}\zeta(3)]\ln\frac{m_\mu}{m_e}+\tfrac{1}{3}\ln^2\frac{m_\mu}{m_e}\right]\left[\frac{\alpha}{\pi}\right]^4=7.1404\left[\frac{\alpha}{\pi}\right]^4. \quad \text{(A18)}$$

Note that (A17) and (A18) have no undetermined constants. On the other hand, numerically integrating the exact expressions (2.2) and (2.7) we found

$$a_{(2;2:2:2)}=a[\text{Fig 2(a)}]=7.2237(13)\left[\frac{\alpha}{\pi}\right]^4, \quad \text{(2.3')}$$

$$a_{(2;2:4)}=a[\text{Fig 3(a)}]=7.1289(23)\left[\frac{\alpha}{\pi}\right]^4, \quad \text{(2.8')}$$

which are consistent with (A17) and (A18), respectively, within the uncertainty of the order of $(m_e/m_\mu)\ln(m_\mu/m_e)$.

The complete contribution to a_∞ from the proper sixth-order vacuum-polarization insertions [eighteen diagrams of Figs. 4(a) and 5] is given in terms of one unknown parameter a_3, the constant term in the asymptotic vacuum polarization in the sixth order:[31]

$$a^\infty_{(2;6)}=a^\infty[\text{Fig. 4(a)+Fig. 5}]$$
$$=\left[-\tfrac{1}{2}a_3+\tfrac{287}{384}+\frac{\pi^2}{72}-\tfrac{5}{12}\zeta(3)+[-\tfrac{67}{96}+\tfrac{1}{3}\zeta(3)]\ln\frac{m_\mu}{m_e}+\tfrac{1}{12}\ln^2\frac{m_\mu}{m_e}\right]\left[\frac{\alpha}{\pi}\right]^4$$
$$=(-\tfrac{1}{2}a_3+1.167729)\left[\frac{\alpha}{\pi}\right]^4. \quad \text{(A19)}$$

Comparing this with the exact result obtained in Sec. II:

$$a_{(2;6)} = a[\text{Fig. } 4(a) + \text{Fig. } 5] = 0.647\,1(203)\left[\frac{\alpha}{\pi}\right]^4, \quad \text{(A20)}$$

we find the unknown coefficient a_3 to be

$$a_3 = 1.041(41) + O\left[\frac{m_e}{m_\mu}\ln\frac{m_\mu}{m_e}\right]. \quad \text{(A21)}$$

We now consider the contribution to a_∞ from the set of 42 eighth-order diagrams generated by inserting proper fourth-order electron vacuum-polarization diagrams into fourth-order muon vertices. The diagrams that belong to this set are those shown in Fig. 3(b) and those represented by the eighth-order muon self-energy diagrams in Figs. 8(a), 8(b'), and 8(b'').

Let us denote by $K^{(4)}(t)$ the anomaly due to fourth-order muon vertex diagrams with one heavy photon of mass squared t. Analytic properties of $K^{(4)}(t)$ allow one to write[31]

$$K^{(4)}(t) = \int_{-\infty}^{0} dt' \frac{1}{t'-t}\frac{1}{\pi}\mathrm{Im}K^{(4)}(t'). \quad \text{(A22)}$$

Introducing the notation

$$\frac{1}{\pi}\mathrm{Im}K^{(4)}(t) = -k^{(4)}\left[-\frac{t}{m_\mu^2}\right]\left[\frac{\alpha}{\pi}\right]^2 \quad (t<0), \quad \text{(A23)}$$

the contribution to a_∞ from the class of digrams under consideration can be written as

$$a_{(4;4)}^{\infty} = \left[\frac{\alpha}{\pi}\right]^2 \int_0^\infty \frac{dy}{y} k^{(4)}(y)\left[d_R^\infty\left[-y\frac{m_\mu^2}{m_e^2}\right]-1\right]_{(4)}. \quad \text{(A24)}$$

Inserting the fourth-order contribution to the asymptotic propagator and defining the integrals

$$I_N = \int_0^\infty \frac{dy}{y} k^{(4)}(y)\ln^N y \quad (N=0,1), \quad \text{(A25)}$$

we may write Eq. (A24) as

$$a_{(4;4)}^{\infty} = \left[-a_2 I_0 - b_2 I_1 - 2b_2 I_0 \ln\frac{m_\mu}{m_e}\right]\left[\frac{\alpha}{\pi}\right]^4. \quad \text{(A26)}$$

The value of the integral I_0 is given by[31]

$$I_0 = 2\left[\tfrac{197}{144} + \frac{\pi^2}{12} - \frac{\pi^2}{2}\ln 2 + \tfrac{3}{4}\zeta(3)\right], \quad \text{(A27)}$$

which is 2 times the fourth-order electron anomaly $a_e^{(4)}$.

The value of I_1 is not known analytically. However, it can be determined from

$$a_{(4;2)}^{\infty} = \left[-a_1 I_0 - b_1 I_1 - 2b_1 I_0 \ln\frac{m_\mu}{m_e}\right]\left[\frac{\alpha}{\pi}\right]^3, \quad \text{(A28)}$$

where $a_{(4;2)}$ is the sixth-order contribution to the muon anomaly obtained by inserting a second-order electron vacuum-polarization loop into the fourth-order muon vertices. Using the values listed in Table VI we obtain

$$a_{(4;2)} = -2.294\,4(12)\left[\frac{\alpha}{\pi}\right]^3, \quad \text{(A29)}$$

which leads to

$$I_1 = -0.972\,9(36). \quad \text{(A30)}$$

We note that I_1 is equal to $3a_e^{(4)}$ within the numerical precision. (Could this be exact?) Substituting (A27) and (A30) into (A26), and taking (A14) into account, we find

$$a_{(4;4)}^{\infty} = -2.647\,4(9)\left[\frac{\alpha}{\pi}\right]^4, \quad \text{(A31)}$$

which is consistent with the numerically obtained "exact" result

$$a_{(4;4)} = a[\text{Fig } 3(b) + \text{Figs. } 8(a), 8(b'), 8(b'')] = -2.666\,9(45)\left[\frac{\alpha}{\pi}\right]^4 \quad \text{(A32)}$$

within an uncertainty of order $(m_e/m_\mu)\ln(m_\mu/m_e)$.

The results (A31) and (A32) disagree strongly with the result (5.11) of Ref. 31. The source of disagreement is traced to an error in formula (5.10) of this reference. Unfortunately it has not been fully corrected in the erratum.

*Present address: Physics Department, Institute R. Boskovic, 41001 Zagreb, Yugoslavia.

†Present address: Physics Department, Nara Women's University, Nara 630, Japan.

[1]T. Kinoshita, B. Nizic, and Y. Okamoto, Phys. Rev. Lett. **52**, 717 (1984).

[2]For a review of this subject, see L. Lyons, in Prog. Part. Nucl. Phys. **10**, 227 (1983). See also F. M. Renard, Phys. Lett. **116B**, 264 (1982).

[3]See, for instance, J. A. Grifols, A. Mendez, and J. Sola, Phys. Rev. Lett. **57**, 2348 (1986), and numerous references quoted there.

[4]T. Kinoshita, B. Nizic, and Y. Okamoto, Phys. Rev. D **31**, 2108 (1985).

[5]T. Kinoshita and W. B. Lindquist, Phys. Rev. Lett. **47**, 1573 (1981). See Ref. 16 for recent improvements.

[6]B. E. Lautrup and E. de Rafael, Phys. Rev. **174**, 1835 (1968).

[7]Particle Data Group, G. P. Yost *et al.*, Phys. Lett. B **204**, 1 (1988).

[8]H. Suura and E. Wichmann, Phys. Rev. **105**, 1930 (1957); A. Peterman, *ibid.* **105**, 1931 (1957); H. H. Elend, Phys. Lett. **20**, 682 (1966); **21**, 720 (1966); G. W. Erickson and H. H. T. Liu, Report No. UCD-CNL-81, 1968 (unpublished).

[9]The sixth-order results are summarized in J. Calmet *et al.*, Rev. Mod. Phys. **49**, 21 (1977).

[10]J. Aldins, S. Brodsky, A. Dufner, and T. Kinoshita, Phys. Rev. D **1**, 2378 (1970).

[11]G. P. Lepage, J. Comput. Phys. **27**, 192 (1978).

[12]T. Kinoshita, Phys. Rev. Lett. **61**, 2898 (1988).
[13]M. A. Samuel and C. Chlouber, Phys. Rev. Lett. **36**, 442 (1976).
[14]T. Kinoshita, Phys. Rev. D **40**, 1323 (1989).
[15]M. E. Cage *et al.*, IEEE Trans. Instrum. Meas. **38**, 284 (1989).
[16]T. Kinoshita, Metrologia **25**, 233 (1988). Further improvement can be found in T. Kinoshita and W. B. Lindquist (unpublished).
[17]For other estimates of $a_\mu^{\rm had}$, see J. A. Casas, C. Lopez, and F. J. Yndurain, Phys. Rev. D **32**, 736 (1985); L. M. Kurdadze *et al.*, Yad. Fiz. **40**, 451 (1984) [Sov. J. Nucl. Phys. **40**, 286 (1984)].
[18]R. Jackiw and S. Weinberg, Phys. Rev. D **5**, 2473 (1972); I. Bars and M. Yoshimura, *ibid.* **6**, 374 (1972); K. Fujikawa, B. W. Lee, and A. I. Sanda, *ibid.* **6**, 2923 (1972); W. A. Bardeen, R. Gastmans, and B. E. Lautrup, Nucl. Phys. **B46**, 319 (1972).
[19]J. Lee-Franzini, in *Proceedings of the XXIV International Conference on High Energy Physics,* Munich, West Germany, 1988, edited by R. Kotthaus and J. H. Kühn (Springer, Berlin, 1989), pp. 1432–1440.
[20]J. Bailey *et al.*, Phys. Lett. **68B**, 191 (1977); F. J. M. Farley and E. Picasso, Annu. Rev. Nucl. Sci. **29**, 243 (1979).
[21]V. W. Hughes and T. Kinoshita, Comments Nucl. Part. Phys. **14**, 341 (1985); M. Greco, Frascati Report No. LNF-88/24(P), 1988 (unpublished).
[22]T. Kinoshita and W. B. Lindquist, Phys. Rev. D **27**, 867 (1983).
[23]For a description of RIWIAD see, for instance, B. E. Lautrup, in *Proceedings of the Second Colloquium in Advanced Computer Methods in Theoretical Physics,* Marseille, France, 1971, edited by A. Visconti (University of Marseille, Marseille, 1971).
[24]T. Kinoshita and W. B. Lindquist, Phys. Rev. D **27**, 853 (1983).
[25]Throughout this paper residual renormalization terms are treated uniformly according to the convention adopted in Ref. 27. This means that group I and group II are treated differently from the conventions of Refs. 22 and 26. This is done to achieve internal consistency and avoid unnecessary confusion. Unfortunately we ourselves were confused in earlier drafts in this paper, and reported a wrong value for $a_\mu^{(8)}$ in the Cornell Report No. CLNS 88/894 (unpublished).
[26]T. Kinoshita and W. B. Lindquist, Phys. Rev. D **27**, 877 (1983).
[27]T. Kinoshita and W. B. Lindquist, Phys. Rev. D **27**, 886 (1983).
[28]Concerning the necessity of quadruple precision for some Feynman integrals, see Ref. 29.
[29]T. Kinoshita and W. B. Lindquist, Phys. Rev. D **39**, 2407 (1989).
[30]T. Kinoshita, Nuovo Cimento **B51**, 140 (1967).
[31]B. E. Lautrup and E. de Rafael, Nucl. Phys. **B70**, 317 (1974); **B78**, 576(E) (1974).
[32]E. de Rafael and J. L. Rosner, Ann. Phys. (N.Y.) **82**, 369 (1974).
[33]B. E. Lautrup and E. de Rafael, Phys. Rev. **174**, 1835 (1968); R. Barbieri and E. Remiddi, Nucl. Phys. **B90**, 233 (1975).
[34]S. L. Adler, Phys. Rev. D **5**, 3021 (1972).